UCLA
UCLA Electronic Theses and Dissertations

Title

Investigations into Wnt modulation of p27(KIP1) turnover and the E3 ligase substrate adaptor DDB1 and CUL4 Associated Factor 4

Permalink

https://escholarship.org/uc/item/3dp9r8zf

Author

Deng, Qiming

Publication Date

2013

Peer reviewed|Thesis/dissertation

UNIVERSITY OF CALIFORNIA

Los Angeles

Investigations into Wnt modulation of p27(KIP1) turnover

and the E3 ligase substrate adaptor DDB1 and CUL4 Associated Factor 4

A thesis submitted in partial satisfaction

of the requirements for the degree Master of Science

in Biological Chemistry

by

Qiming Deng

2013

ABSTRACT OF THE THESIS

Investigations into Wnt modulation of p27(KIP1) turnover

and the E3 ligase substrate adaptor DDB1 and CUL4 Associated Factor 4

by

Qiming Deng

Master of Science in Biological Chemistry

University of California, Los Angeles, 2013

Professor Timothy F. Lane, Chair

ABSTRACT

Wnt signaling plays a major role in cell proliferation, cell fate, and stem cell maintenance. Its regulatory function is achieved through the induction of numerous downstream Wnt target genes. Relatively little work has focused on the influences of Wnt signaling on the ubiquitin proteasome system. Our work has examined Wnt transcriptional modulation of WD40 genes with potential function as E3 ligase substrate adaptors, and we present evidence that DCAF4 is a Wnt target gene. We have confirmed DCAF4 as a component of the CUL4 RING E3 ligase (CRL4) associated protein consistent with previous research. Our research has uncovered differential CRL4 binding amongst its splicing variants and an N-terminal domain that appears to regulate this interaction. We have also revealed a number of novel DCAF4 associated proteins by MudPit mass spectrometry analysis of DCAF4 with the most interesting being components of the prefoldin and BAT3 complexes.

The thesis of Qiming Deng is approved.

John J. Colicelli

Kenneth Bradley

Timothy F. Lane, committee chair

University of California, Los Angeles

2013

Dedicated to my loving wife and to my wonderful kids.

TABLE OF CONTENTS

CHAPTER 1 Introduction

1.1 Wnts

Wnts comprise a family of 19 secreted glycoproteins that is found in many species ranging in complexity from fruit flies to humans. The first Wnt was originally dubbed *wingless (wg)* in 1973 for the eponymous "wingless" mutation that interfered with wing and haltere development in *Drosophila* [1]. The significance of *wingless* would not stay localized to wing disc development as further research revealed additional roles in segment polarity [2]. A decade later, Roel Nusse and Harold Varmus first identified its mammalian homolog Int1 in mice as a proto-oncogene that generated mammary tumors following activation caused by the integration of the retrovirus MMTV in its vicinity [3]. Other investigations found that injection of mouse Int1 mRNA into fertilized *Xenopus* eggs led to the duplication of the dorsal axis that formed bifurcated neural plates [4].

These discoveries highlighted the importance of Wnt signaling to body patterning and development while also demonstrating its relevance to oncogenesis. It is not surprising that Wnts regulate such essential pathways given that they have ancient origins tracing back to the evolution of multi-cellular organisms [5]. Since then, Wnts appear to have undergone rounds of duplication and differentiation, which have been hypothesized to reflect the increases in body patterning complexity throughout metazoan evolution [6]. These pioneering studies laid the groundwork for the explosion of research that followed, which has linked Wnts to diverse developmental and physiological processes and their underlying molecular pathways.

1.2 Canonical Wnt pathway

The canonical Wnt pathway is activated when extracellular WNT proteins bind to target receptors comprised of members from the Frizzled family and LRP5/6 on the cell surface. The first Frizzled was originally discovered as a regulator of planar polarity when mutations caused altered cell orientation in regions of the adult *Drosophila* cuticle [7]. Frizzled was further characterized as having seven transmembrane and a cysteine-rich extracellular domain [8]. The connection to Wnt was not made until *Drosophila* Frizzled 2 homolog was cloned and found to exhibit an early segment polarity phenotype shared with *wingless* and *disheveled* [9]. After the discovery that beta catenin, whose *Drosophila* homolog *armadillo* functioned in segment polarity much like wingless, was associated with the adhesion gene P-cadherin, a model soon emerged that implicated Wnt signaling in cell adhesion and its growth-related functions [10-12].

The LRP co-receptors were discovered later and found to physically interact with Frizzled and mediate Wnt signaling [13]. While Frizzled recruits Disheveled to the intracellular side of the cell membrane, LRP plays a critical role in binding GSK3 beta and AXIN after its cytoplasmic tail is phosphorylated in response to WNT ligand [14, 15]. Eventually, it became apparent that GSK3 beta was in complex with other Wnt pathway components AXIN and APC; they comprised the core of a "destruction complex," which phosphorylates cytoplasmic beta-catenin, thereby marking it for polyubiquitination and subsequent degradation by the proteasome [16]. Frizzled/LRP activation leads to the reorganization and recruitment of this destruction complex to the cell membrane, thereby inactivating GSK3 beta's ability to phosphorylate and target beta catenin to the ubiquitin proteasome system [17].
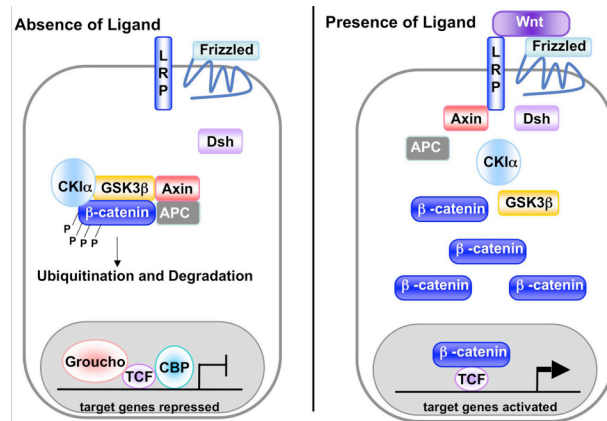
Figure 1.1 Canonical Wnt signaling pathway.
In the absence of WNT ligand, cytosolic beta catenin (CTNN1B) is phosphorylated by the destruction complex composed of GSK3B, CKI, APC, and AXIN. Phosphorylated CTNN1B is then polyubiquityled by E3 ligase activity and degraded by the proteasome. Upon ligand binding to the Frizzled and LRP co-receptors, the destruction complex is reorganized and its kinase activity inhibited. This leads to beta catenin stabilization and translocation into the nucleus where it binds TCF/LEF proteins to activate transcription of WNT target genes

As shown in Figure 1.1, in the absence of Wnt signaling, cytoplasmic beta catenin is found associated with cadherin complexes at the cell membrane or with the "destruction complex" [18]. Upon Wnt-induced GSK3 beta repression, beta catenin is stabilized and translocates into the nucleus. A key piece of the canonical Wnt pathway puzzle was found when beta catenin was discovered to bind TCF/LEF1 transcription factors [19]. Once in the nucleus, beta catenin forms a complex with TCF/LEF1 and other co-factors, activating them for transcription of target genes involved in various processes that include body patterning, stem cell maintenance, and tissue differentiation and proliferation [16].

1.3 Wnt signaling in cancer

Gene	Type of mutation	Primary tissues	Number of mutated samples	% mutated	Total samples
APC	Primarily frameshift and deletion mutations leading to compromised ability to degrade CTNNB1	Large intestine	2152	39%	5517
		Stomach	129	15%	214
		Soft tissue	50	12%	430
		Small intestine	34	16%	214
		Pancreas	26	14%	184
		Liver	11	12%	94
CTNNB1	Mutations in CTNNB1 cluster around the amino-terminus and prevent the phosphorylation of amino acids, S33, S37, T41 and S45, resulting in impaired degradation of CTNNB1	Liver	907	23%	3933
		Soft tissue	673	42%	1601
		Endometrium	218	20%	1098
		Kidney	168	14%	1225
		Pancreas	125	26%	476
		Ovary	104	11%	913
		Adrenal gland	100	19%	534
		Pituitary	86	24%	360
		Biliary tract	43	10%	433
AXIN1	Many mutations prevent AXIN1 from acting as a scaffold to degrade CTNNB1	Biliary tract	10	38%	26
		Liver	49	11%	448
WTX (also known as FAM123B)	Predicted to be loss-of-function mutations	Kidney	125	13%	949
		Large intestine	19	13%	151
TCF7L2	Unknown	Large intestine	13	28%	47

Anastas & Moon 2013 (Ref 26)

Table 1.1 Somatic Wnt pathway mutations in human cancers.

Overactive Wnt signaling has been implicated in a number of tumor types since its discovery as a proto-oncogene in mice (Table 1.1). Perhaps the most compelling evidence for a causal relationship between Wnt signaling and human cancer was first found in colorectal cancer, where inherited mutations in the Wnt pathway led to aberrant beta catenin activation and tumorigenesis [20, 21]. Indeed, the APC gene was first isolated as a result of these efforts to identify the genetic mutations underlying the hereditary colorectal cancer adenomatous polyposis coli [22]. APC was inactivated by nucleotide substitutions and deletions that created premature stop codons or frameshift deletion mutations, which supported the model that APC was a tumor suppressor [22]. These findings were corroborated by the Min (multiple intestinal neoplasia) mouse lineage that has an inherited autosomal dominant predisposition for developing colorectal tumors.

The Min locus was discovered to be tightly mapped to an APC gene with a nonsense mutation [23]. Mutations to Wnt pathway components beta catenin and AXIN1 were also linked to tumorigenesis in a variety of tissues including the intestines, stomach, pancreas, liver, and soft tissues [24-26]. Such mutations occur with great frequency in numerous cancers as both inherited germline mutations and somatic mutations [26].

Although aberrations to the Wnt pathway clearly have the capacity to initiate the proliferation necessary for tumorigenesis, studies have identified roles in additional cancer-related functions that include survival, senescence, cell migration, and invasiveness, which resembles the epithelial-to-mesenchymal transition that drives metastasis [26]. However, not all Wnts are proto-oncogenic, and there is data to suggest anti-tumorigenic potential depending on the molecular and cellular context [26]. One way to assess this is to introduce Wnts in cultured cells and assess morphological transformation. Such an assay showed that Wnt1, Wnt3A, and Wnt7A had high transforming capability in contrast to Wnt4, Wnt5A, and Wnt6 that completely failed to induce transformation in C57MG mouse mammary epithelial cells [27]. Wnt7A is especially interesting in that it drives proliferation and beta catenin dependent transcription of Wnt target genes in ovarian cancer cells, but represses growth and fails to activate canonical Wnt signaling in leukemia and Jurkat cells respectively [28, 29]. The importance of cellular context was further established when co-transfection of Wnt7A with either Frizzled 5 or Frizzled 10 receptor led to activation of the canonical beta-catenin pathway or the noncanonical JNK-mediated pathway respectively [30]. Only activation of the canonical pathway via Frizzled 5 induced proliferation, illustrating how

distinct sets of Wnt receptors could lead to dramatically divergent phenotypic responses to a particular Wnt ligand [30].

1.4 Wnt signaling & cancer stem cells

Cancer cells are typically composed of a heterogeneous population with a core subset of cells that possess the stem cell's ability to self-renew. Conventional treatments that kill off the vast majority of a tumor may still fail to eliminate the cancer if some of these stem-like cells survive due to their ability to reconstitute the tumor. Furthermore, because these cells undergo division more infrequently they are more likely to survive treatments that target cell proliferation. An important stem cell characteristic is the expression of ABC type transporters that confer protection from toxins by export, and in fact, this ability has been utilized to isolate stem cell side populations with flow cytometry by measuring their ability to efflux Hoechst dye [31]. Cancer stem cells exploit this pathway to confer resistance to chemotherapeutic drugs. Therefore, they present attractive candidates for targeted therapeutic research.

Because the Wnt pathway is a known contributor to adult stem cell maintenance and differentiation, it was theorized to fulfill a similar function in cancer stem cells. Wnt modulation of stem cells occurs through the control it exercises over target gene expression. In one study, C-terminal deletions to beta catenin that eliminated binding of transcription co-factors allowed for non-transcription related functions to be retained [32]. With the defect solely targeting transcription, mutant beta catenin resulted in defective embryonic neural progenitors and embryonic lethality during gastrulation [32]. Known cofactors Kindlin2 and BCL9 were found to associate with beta catenin to effect

transcription of target genes necessary for epithelial-to-mesenchymal transition and cancer stem cells [33, 34].

Beta catenin activation also appears to cooperate with the pluripotency modulator Klf4 to drive expression of the telomerase subunit Tert. This was demonstrated in comparisons between beta catenin deficient mouse embryonic stem cells with short telomeres and active beta catenin mouse ES cells with long telomeres [35]. Telomerase activity is critical for maintaining the telomere structures that cap chromosomes to provide genomic stability, and the shortening of telomeres with each round of cell division limit the possible number of cell divisions before DNA damage leads to senescence or apoptosis [36]. Stem cells have extra long telomeres that progressively shorten as they differentiate and age, but cancer stem cells regain the ability to maintain their telomeres [36]. Since aberrant telomerase activity has been associated with tumorigenicity and offers cancer cells a pathway for overcoming senescence and apoptosis, the Wnt pathway could provide a therapeutic approach for targeting the cancer stem cells that have the ability to regenerate tumors.

1.5 Wnt & the ubiquitin proteasome system

Because canonical Wnt signaling acts through transcriptional modulation of numerous Wnt target genes with roles in key regulatory pathways, it is unsurprising that Wnt has been linked to such wide-ranging cellular and developmental phenomenon. One of these pathways is the ubiquitin proteasome system (UPS).
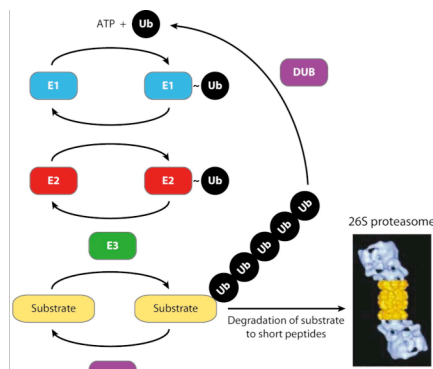
Figure 1.2 Ubiquitin proteasome pathway
Substrate ubiquitylation takes place through a series of enzymatic steps involving ubiquitin
activation by the E1, conjugation by the E2, and substrate targeting by the E3 enzymes.

Figure 1.2A diagrams the ubiquitylation process, which is a post-translational
modification carried out in a series of enzymatic steps by the E1, E2, and E3 ubiquitin
ligase [37]. First, ubiquitin activation is catalyzed by the E1 activating enzyme in an
ATP-dependent step as it forms a high energy thioester bond with the 76 amino acid
ubiquitin molecule. The activated ubiquitin is next transferred to a cognate E2
conjugating enzyme. The E2 enzyme can then engage one of a vast array of E3 ubiquitin
ligases to ubiquitylate the target substrate [38]. E3 ligases are characterized by the
presence of specific functional domains including the HECT, U-box, and RING domains.
Substrate ubiquitylation is directly catalyzed by HECT E3 ligases with the ubiquitin
transferred from the E3 to the substrate. In the case of the RING E3 ligases, the E2-
ubiquitin conjugate is bound by the E3 ligase, which indirectly catalyzes ubiquitylation
by mediating the transfer of ubiquitin from the E2 to a substrate lysine. U-box E3 ligases
share a 70aa U-box motif, which is a modified RING domain, and also mediate
ubiquitylation indirectly by physically coordinating E2-Ub and substrates [39].

Substrates can be tagged with single ubiquitin or polymeric ubiquitin chains at
one or more lysines. Adding to the complexity is the presence of seven lysines and the N-

terminal residue on the ubiquitin molecule itself, which can each be used for the attachment of additional ubiquitin [40]. An ubiquitin chain can be homogeneous with its monomers linked via the same lysine residue, while mixed topologies are characterized by alternating linkages or even multiple linkages within the same ubiquitin to form branched chains [40]. The various forms of mono- and polyubiquitylation play essential roles in cellular processes that include cell cycle regulation, antigen processing, DNA transcription and repair, apoptosis, receptor endocytosis, and protein quality control pathways [41-46].

In particular, polyubiqitination of intracellular proteins by ubiquitin E3 ligases marks them for eventual turnover or sequestration [47]. The UPS works in conjunction with autophagy, lysosomes, and proteases to carry out a significant portion of the regulated degradation of intracellular proteins [37]. Protein turnover is critically important since many proteins have key functions such as apoptosis, DNA replication, and cell cycle progression that require they be tightly regulated, and some have half-lives that can be measured in just minutes [37]. Furthermore, a percentage of proteins become misfolded or damaged during their lifespan, and even newly synthesized proteins can fail to fold properly. These abnormal proteins could disrupt the various pathways with which they are associated, so it is crucial that they are accurately and efficiently targeted for degradation to minimize cellular damage. Indeed, the failure of the UPS to effectively degrade substrates has been linked to disease and aging.

For example, Parkinson's disease is characterized by the presence of Lewy bodies in neuronal cells. These inclusions are fibrillar aggregates enriched with alpha-synuclein and abnormal neurofilaments, and include components of the UPS such as ubiquitin, the

proteasome, and the parkin E3 ligase [48]. It is believed that Lewy bodies represent a response to an overabundance of aggregation-prone proteins, which exceeds the capacity of the cell's proteolytic machinery. Indeed, mutations to the parkin E3 ligase are responsible for juvenile early-onset Parkinsons disease, and the protein Synphilin-1, whose overexpression causes the formation of Lewy body-like inclusions, is an ubiquitylation target of the Parkin, SIAH, and Dorfin E3 ligases [49].

A significant proportion of cellular proteins are estimated to be recycled through the ubiquitin proteasome system [50]. Indeed, the canonical Wnt signaling molecule beta catenin is itself regulated through targeted polyubiquitylation by the $SCF^{\beta\text{-}TrCP}$ E3 ligase and subsequent proteasomal degradation in the absence of Wnt pathway activation [51]. Further research has revealed additional mechanisms by which ubiquitylation modulates Wnt activity. While cytosolic beta catenin turnover is well characterized, recent research has found that activated nuclear beta catenin is regulated by the E3 ligase c-Cbl in endothelial cells [52]. Wnt signaling appears to drive the nuclear translocation of c-Cbl where it ubiquitylates beta catenin in a negative feedback mechanism to suppress activation of Wnt target genes [52]. Conversely, beta catenin ubiquitylation by the EDD E3 ligase leads to enhanced stability and nuclear translocation [53]. The Wnt pathway mediator Disheveled2 has also been shown to be ubiquitin regulated. In fact, Dvl2's crucial role in relaying extracellular Wnt ligand-receptor binding to intracellular effectors has made it a rather popular regulatory target as evidenced from its turnover by the E3 ligases NEDD4L and KLHL12 [54-56]. The HECT domain-containing E3 ligase NEDD4L, which not coincidentally has a regulatory role regarding cell polarity, targets Dvl2 for ubiquitin-dependent proteasomal degradation with downstream effects on beta

10

catenin levels [54]. KLHL12 is also observed to interact with Dvl2 in a Wnt-dependent manner [56]. Such studies have greatly expanded our understanding of the intricacies of Wnt signaling and its relationship to the ubiquitin proteasome system. However, much work has focused on UPS modulation of Wnt signaling, while less attention has been devoted to Wnt regulation of E3 ligase activity regarding other pathways.

CHAPTER 2 Evaluation of Wnt10b-driven p27 turnover

2.1 Background

Wnt10b & breast cancer

Researchers have found that one major molecular pathway misregulated in a significant percentage of breast carcinomas is the canonical Wnt signaling pathway [57]. Multiple lines of evidence have linked Wnt signaling to breast cancer since the discovery that ectopic expression of Wnt1 in the mammary gland induced adenocarcinoma formation [3]. While normal Wnt1 expression was limited to postmeiotic male germ cells and the neural tube during embryogenesis, evidence has found Wnt10b, which is normally expressed during mammary gland development, to have similarly high transforming potential [58, 59]. Downstream targets of the canonical Wnt signaling pathway have also been implicated. Cyclin D1, a breast cancer marker overexpressed in 50% of patients, is transcriptionally regulated by beta-catenin [57]. Additionally, both beta-catenin and Cyclin D1 were found to independently correlate with poor prognosis [57]. In contrast to erbB2-driven mammary tumors, which can be inhibited via cyclin D1 depletion in mouse models, Wnt signaling modulates additional isoforms and thus makes a more difficult target for potential drugs [60].

In particular, Wnt signaling may be of relevance with regards to a distinct category of difficult to treat breast cancers that are described as "triple-negative" for not expressing estrogen and progesterone receptors and for lacking over-expression of human epidermal growth factor receptor 2 [61]. Triple negative breast cancers are typically characterized by a basal molecular subtype, early and aggressive metastasis, and poor outcome [61]. The lack of obvious molecular pathways presents a serious challenge for

targeted therapies. Interestingly, Wnt pathway activation has been found to correlate with the triple-negative breast carcinomas and its poor prognosis [62]. Furthermore, Wnt receptor Frizzled7 and co-receptor LRP6 tend to be upregulated in this subset of cancers and make strong candidates for therapeutic targets [63-66]. Together, the body of evidence makes a compelling argument for a role involving Wnt signaling in the triple negative subtype of breast cancer.

Wnt10b regulation of p27

Despite the significant quantity of correlative data, much is still unknown regarding the mechanisms by which Wnt signaling transforms mammary tissue. Evidence has suggested that the nature of Wnt's transforming potential lies within its role in stem cell maintenance and differentiation [67]. Given that Wnt signaling has been found to be essential in a variety of stem cell niches, it is not surprising that Wnt is also implicated in mammary stem cell activity [67, 68]. While much research has focused on direct transcriptional targets of Wnt signaling, our lab has also examined post-translational targets in mammary epithelial cells. A screen for post-translational targets identified Wnt10b induced downregulation of p27^{KIP1}, a tumor suppressor protein that works by binding to and inactivating Cdk2-cyclin E [69, 70]. Figure 2.1 shows a comparison of mammary tumor tissue paraffin sections from MMTV-ErbB2 and Wnt10b transgenic mice. The cell cycle inhibitor p27 is noticeably absent in the Wnt10b tumor section. This relationship also holds in non-tumorigenic mammary gland tissue with decreasing p27 protein staining correlating with increased Wnt10b expression (Figure 2.1B).

13
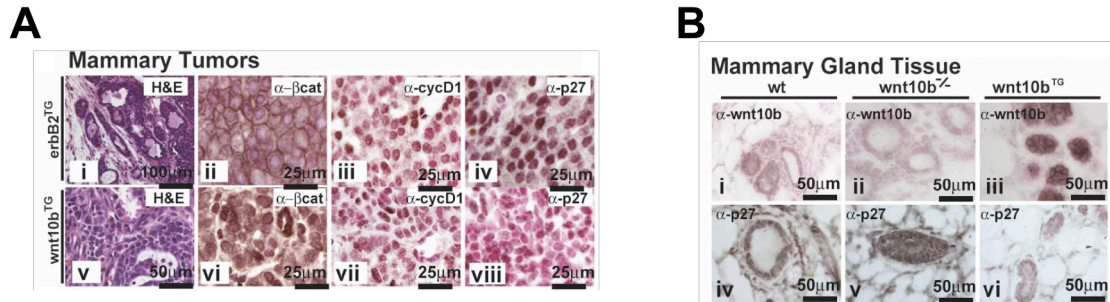
A Mammary Tumors

B Mammary Gland Tissue

Figure 2.1 p27 (CDKN1B) protein is inversely correlated with WNT10B protein levels in mammary tumors and mammary gland tissue.
(A) Paraffin sections from *Wnt10b* and *ErbB2* transgenic mouse mammary tumor tissue were stained with H&E to reveal overall cellular morphology. Sections were also stained by IHC for beta catenin (CTNN1B) to demonstrate nuclear localization in the *Wnt10b* transgenic tissue, cyclin D1 (CCND1), and the cell cycle inhibitor CDKN1B. Nuclear fast red was used as a counterstain. (B) Nontransformed mammary gland tissue from wild-type, wnt10b null, and wnt10b transgenic mice were analyzed by IHC for WNT10B and CDKN1B protein expression.

P27 accumulates in growth-arrested cells at G0/G1, and its inhibition of Cdk2-cyclin E prevents progression into the S phase [71]. Release from cell cycle arrest leads to significant p27 turnover by late G1 and S phase [72]. P27 knockout mice are 30% larger than wild-type, have higher Cdk activity, and spontaneously grow tumors [69]. However, p27 is infrequently mutated in human cancers, and regulation tends to be post-translational rather than at the transcriptional level [69]. Phosphorylation & polyubiquitination pathways target p27 for proteasomal degradation [69, 71].

Several pathways mediating p27 turnover have thus far been characterized [73-75]. The best understood mechanism occurs through the SCF^{SKP2} E3 ligase complex (Figure 2.2). This complex recognizes p27 during late G1 and S phase, and targets it for proteasomal degradation [75]. P27 is marked first by cdk2-cyclin A/E-mediated phosphorylation of the T187 residue, which allows recognition by the F-box protein Skp2

[75]. Skp2 acts as the substrate recognition component that targets the SCF complex to
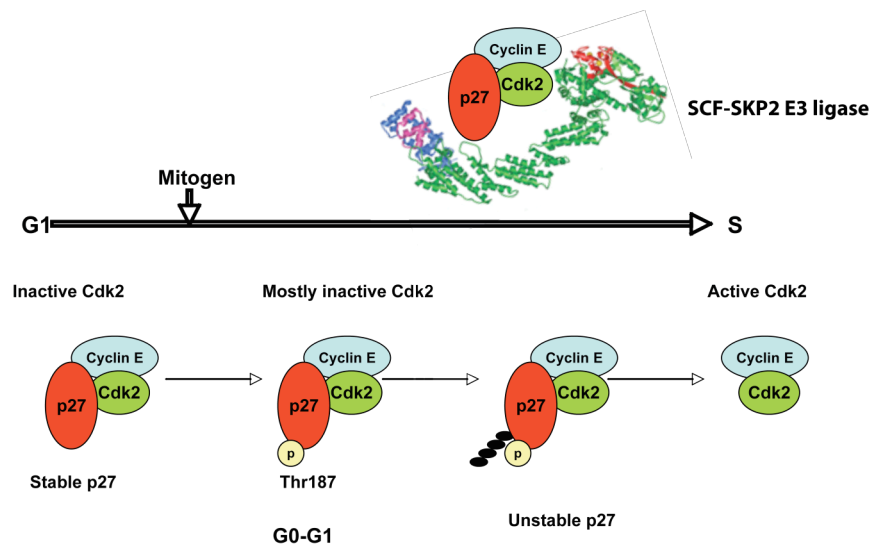
Figure 2.2 The cell cycle inhibitor p27 (CDKN1B) regulates G1-S phase transition and is targeted for proteasomal turnover by the SCF E3 ligase.
CDKN1B stably binds CDK2/CCNE complexes in G1, inhibiting phosphorylation of downstream target RB1. Following T187 phosphorylation, CDKN1B is targeted for polyubiquitylation by the SCF complex and degraded. The release of CDK2/CCNE repression allows for phosphorylation of Rb and other target genes involved in the G1-S phase transition.

p27 [76]. Once polyubiquitinated by the SCF complex, p27 is proteolytically degraded by the 26S proteasome. The turnover of p27 then releases the repression of Cdk2-cyclin A/E, allowing the complexes to phosphorylate downstream targets critical for G1-to-S phase transition such as Rb . The importance of Skp2-mediated p27 turnover has been demonstrated in Skp2^{-/-} null mice, which are 30% larger than wild-type littermates and exhibit p27 accumulation [77]. Skp2^{-/-} null MEFs become growth arrested in G1/S phase, presumably due to p27 accumulation. Examination of Skp2-/- p27-/- double KO mice showed that the Skp2^{-/-} KO phenotype is rescued by knocking out p27 [78].

Wnt mediated p27 turnover is Skp2 independent and Cullin dependent

Due to its prominent and well-characterized role in p27 turnover, the E3 ligase SCF[SKP2] was hypothesized to be the effector of Wnt induced p27 turnover. However, Wnt
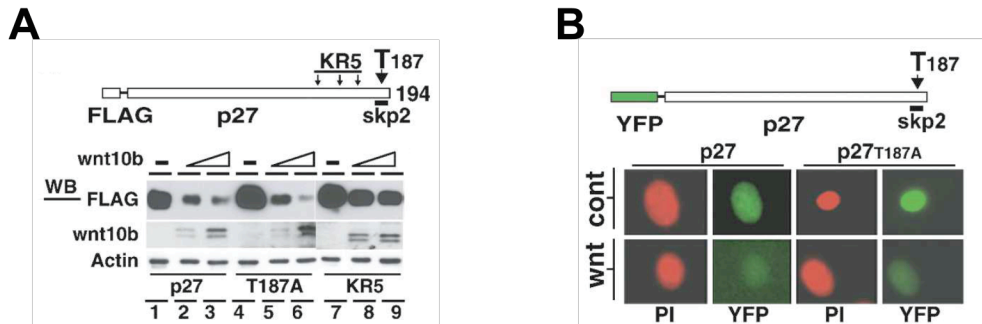
Figure 2.3 WNT10B induced p27 (CDKN1B) proteasomal turnover is SKP2 independent.
(A) FLAG-p27 expression vectors were mutated (T187, KR5 = lysine mutations) and assayed for steady state protein levels when co-transfected with varying amounts of Wnt10b expression vector. (B) The same experiment was performed but using N-terminal YFP fused p27 and analysis by fluoresence microscopy to determine the expression level of p27 when co-transfected with Wnt10b.

pathway activation was capable of turning over p27 in SKP2^{-/-} MEFs [70]. In Figure 2.3, mutating p27 to prevent phosphorylation of its Threonine 187 residue, which targets it for SKP2-mediated polyubiquitylation, also failed to rescue p27 turnover, but mutagenizing multiple lysine residues needed for ubiquitin attachment succeeded in reducing turnover [70]. The subsequent search for an alternate E3 ligase identified the DDB1 CUL4 RING complex (CRL4). Expression of dominant negative CUL4 appeared to counteract p27 turnover, and immunoprecipitated p27 was able to pull down transfected HA-CUL4A [70]. CRL4 utilizes a wide variety of DDB1 and CUL4 Associated Factors (DCAFs) with putative substrate targeting functions, and many more are believed to be unidentified.

Finding the substrate adaptor is especially relevant in the context of cancer biology. Because one third of human breast cancers exhibit an unexplained SKP2-low/p27-low phenotype, elucidating this pathway may reveal the mechanism for p27

turnover in this cancer cluster [79]. These lines of evidence laid the groundwork for our investigation into the p27 targeting subunit of the CUL4 E3 ligase.

Project Aims

A) To validate Wnt-driven p27 turnover

B) To demonstrate p27 co-precipitation with CRL4 components

C) To identify the CRL4 substrate adaptor responsible for targeting p27 for polyubiquitylation

2.2 Materials and Methods

<u>*All vectors and oligos are listed in Appendix Table A.1</u>

FLAG-p27 point mutations

pcDNA3 FLAG-p27wt expression vectors were modified to generate the following point mutations: Y74F, Y88F, Y88F Y89F. Mutagenesis primers were designed with the Quikchange Primer Design online software from Agilent Technologies. PCR mutagenesis of pCMV6-Entry DCAF4 wild-type vectors was carried out using high fidelity Deep Vent polymerase (NEB) for 16 cycles of $95^{o}C$ 1min denaturation, $60^{o}C$ 1min annealing, and 10min $72^{o}C$ extension. The original template vector was eliminated through Dpn I digestion at $37^{o}C$ for 2h. DNA precipitation was carried out by addition of 1X volume of 100% ethanol and 2uL of glycogen, followed by incubation at $-20^{o}C$ for 30min to overnight. Precipitated DNA pellet was centrifuged at 14k rpm for 15min, washed once with 70% ethanol, air dried, and finally dissolved in TE buffer (Qiagen). Aliquots were transformed into TAM1 competent cells and plated on ampicillin agar plates. Colonies were grown in 2YT liquid media 16h at 225rpm $37^{o}C$. Clones were then purified with

17

Qiagen miniprep spin columns and validated by DNA sequencing with CMVf and M13r primers.

Gateway-p27 cloning

We obtained the plasmid components of the Gateway cloning system, which consists of an Entry vector, a pcDNA5 FRT TO destination vector that can be stably integrated into T-Rex cell lines through recombination, and the Flp recombinase expression vector pOG44 (Invitrogen). The Entry vector we obtained already had the ORF insert for wild-type p27. The Gateway system allowed the Entry vector's insert to be efficiently recombined into various destination vectors with experiment specific attributes. In this case, we used LR Clonase to recombine p27wt into a pcDNA5 destination vector that fused the N-terminus of the insert with triple HA and FLAG tags. The vector also had a Flp recombination site (FRT) for recombination into Flp-In™ cell lines containing single FRT sites that restrict integration to a single copy per cell. This methodology minimizes the disruption to endogenous cellular pathways that may be posed by the random integration of multiple copies of the expression vector.

We generated an additional version of this p27 destination vector by introducing the T187A mutation. This was accomplished by first excising the p27 insert from both the pcDNA3 FLAG-p27 vector and the Gateway-p27 destination vector with the restriction enzymes Apa I and Sfb I (NEB). The p27 T187A insert and the Gateway destination backbone were then gel purified and ligated overnight at $16^{\circ}C$ with T4 DNA ligase. To prevent the backbone from re-ligating with itself, it was CIP treated for 30 minutes at $37^{\circ}C$ prior to gel purification. The ligation products were transformed into

TAM1 competent cells. Successful clones were isolated and validated by DNA sequencing.

Cell culture maintenance

Human HEK293T and Flp-In HEK293 T-Rex cells (Invitrogen) were maintained in a humidified atmosphere with 5% CO2 in Dulbecco's Modified Eagle's Medium supplemented with 10% fetal calf serum, 100 U/ml penicillin, and 100 ug/ml streptomycin. The Flp-In HEK293 T-REx cell line stably expressed the Tet repressor protein, which binds to a recognition Tet operator sequence to suppress downstream gene expression in the absence of tetracycline. Included in the vector was a single FRT recombination site for the stable integration of a single copy of a Gateway FRT destination vector.

The Wnt mimetic lithium chloride and its salt control sodium chloride were dissolved in ddH$_2$O and filter sterilized using 0.22 micron PVDF syringe filters to generate 5M stock solutions. The stocks were diluted into media for working concentrations of 20mM. Tetracycline was prepared the same way at 2ug/uL stock and 200ng/mL working concentrations respectively (10,000X dilution). The inhibitor of protein synthesis cycloheximide was prepared at 50mg/mL stock dissolved in DMSO and diluted to 5ug/mL working concentration. The proteasome inhibitor MG132 was prepared at 10mM stock concentration and used at 10uM.

Transfection

293T/T-Rex cell lines were plated at ~50% confluence the day before transfection. Cells were co-transfected with the desired expression vectors and pUC18 carrier DNA using the calcium phosphate protocol. Transfected cells were washed 3X with PBS and given

fresh media after 8h incubation. Downstream analyses by immunofluorescence or Western Blot took place 24-48h following transfection unless stated otherwise.

Stable cell line generation

Gateway-p27wt and T187A stable cell lines were generated by co-transfecting pOG44 Flp Recombinase expression vector with pcDNA5 FRT TO 3HA-3FLAG p27 destination vectors into HEK293 T-Rex cells. The expression of Flp recombinase allows for the recombination between the genomically integrated FRT site in the cell line and the FRT site on the destination vector. The destination vector was also designed so that it contained a hygromycin B resistance gene cassette that was missing the transcription start codon. This start codon was also designed into the FRT recombination site so that only the intended recombination would lead to the active transcription of the hygromybin B resistance gene. Two days following transfection, cells were selected with 200ug/mL Hygromycin B for 2 weeks before surviving colonies were picked and assayed for tetracycline-induced expression by Western Blot. Wnt10b, dominant active beta catenin, and SFB tagged DDB1 stable cell line generation was achieved using identical techniques except cells were selected with 1mg/mL G418 instead of Hygromycin B.

Cell culture treatments

Protein extraction & immunoblotting

Adherent cells were harvested from flat well cell culture plates by scraping or pipetting in ice cold PBS. Pellets were flash frozen in liquid nitrogen and stored at -80C. Cell lysis was achieved by vortexing pellet in ~10X volume EBC lysis buffer (0.5% NP40 150mM NaCl 50mM Tris pH 8.0) supplemented with Roche complete protease inhibitor tablets. Lysate was incubated on ice for 30min while being vortexed regularly. Lysate was then

centrifuged 14k rpm 15min at 4°C to pellet cellular debris. The supernatant was transferred into a new microcentrifuge tube. Protein extracts were mixed with 6X Laemmli buffer supplemented with DTT and then boiled 5min and separated by SDS-PAGE. Separated proteins were then transferred onto PVDF membranes at 22V overnight. Membranes were blocked with 5% milk in TBST buffer for 1h at room temperature. Membranes were incubated with primary antibodies in 3% milk TBST blocking buffer overnight at 4°C, washed 3X in TBST, then blocked with secondary HRP-conjugated antibodies in 5% milk TBST blocking buffer for 1h at room temperature. Following three final washes in TBST, the blots were developed with Supersignal West Pico Stable Peroxide Solution and Luminol Enhancer Solution (Pierce).

Silver staining

Following SDS-PAGE separation of protein extracts, the acrylamide gels were fixed for 1h at room temperature in fix solution (40% methanol, 10% glacial acetic acid), washed in ddH$_2$O twice for 5min, soaked 10min in sensitizing solution (0.02% Na$_2$S$_2$O$_3$), rinsed in ddH$_2$O twice, and then stained with 0.2% silver nitrate solution for 10min. The gels were then soaked in developing solution (6% Na$_2$O$_3$) for 10min and washed one last time in terminating solution (12% glacial acetic acid).

Immunoprecipitation

FLAG-tagged protein lysates were pre-cleared by incubating with GST-sepharose beads for 1h at 4°C while inverting gently. The supernatant was then incubated with anti-FLAG M2 EZView beads (Sigma) overnight at 4°C. Following three washes in IP wash buffer (150mM NaCl 50mM Tris pH 8.0, protease inhibitors), the beads were eluted for 15 minutes at room temperature using FLAG tripeptide elution buffer (FLAG tripeptide

dissolved in EBC lysis buffer). The eluate was combined with 6X Laemmli buffer and boiled for analysis by SDS-PAGE and immunoblotting. Streptavidin purification of SFB-DDB1 was carried out using the FLAG IP protocol but with streptavidin conjugated sepharose beads and an elution buffer containing 2mg/mL biotin.

Batch immunoprecipitation of 3X-HA 3X-FLAG p27 for Mudpit mass spectrometry analysis utilized anti-HA conjugated agarose beads (Roche). The beads (0.5mL) were packed into 2mL disposable polystyrene columns and washed in 5 column volumes of equilibration buffer (20mM Tris, 0.1M NaCl, 0.1mM EDTA pH 7.5). The cell lysate was applied to the gravity column, which was then washed with 20 column volumes of wash buffer (20mM Tris, 0.1M NaCl pH 7.5). Finally, 2 column volumes of elution buffer (1mg/mL HA peptides dissolved in equilibration buffer) were applied to the column, and the elution fractions were collected.

Real time PCR

RNA was purified with the RNeasy plus mini kit (Qiagen) and used to generate cDNA with the high capacity reverse transcription kit (Applied Biosystems). Real time PCR reactions were prepared using SYBR Green qPCR master mix (Veriquest). Primers were designed with the ncbi primer BLAST website to amplify regions of mRNA transcripts between 100-150bp in length (Appendix Table A.1). To minimize interference caused by contaminant genomic DNA, primers were designed to span exon-exon junctions, and primer pairs were separated by intron sequences of at least 1000bp. PCR reactions were run and analyzed on the MX-3000P qPCR system (Agilent Technologies). Samples were run in duplicate, and expression levels were determined by the $\Delta\Delta Ct$ method [80].

2.3 Results

Site mutagenesis of phosphorylation sites have no consistent impact on p27 protein levels

Previously, mutation of the T187 residue on p27 was found to stabilize p27 protein due to the residue's phosphorylation being required for recognition and polyubiquitylation by the SCF^{Skp2} complex [75]. The lack of Skp2 involvement raised the possibility that Wnt driven targeting of p27 may depend upon an alternate phosphorylation site. In breast cancers, estrogen receptor is frequently activated with a mitogenic function, and one of its downstream targets is Src kinase, which in turn can activate receptor tyrosine kinases to stimulate proliferation [81, 82]. Src kinase has been found to phosphorylate p27 at tyrosine residues 74, 88, and 89 with a corresponding effect of decreased p27 association with Cdk2-Cyclin E and reduced stability [81].
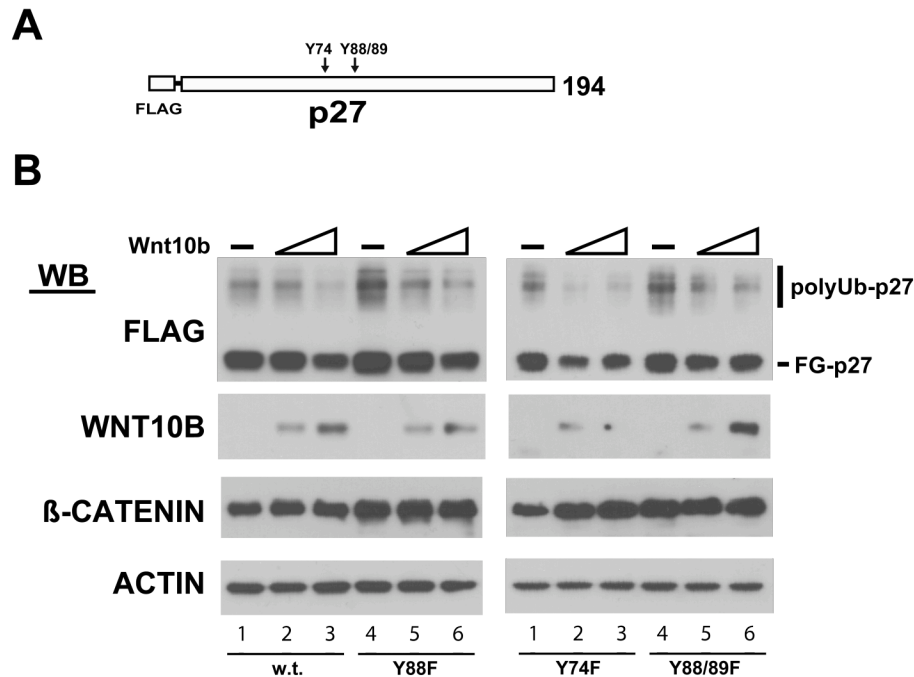
Figure 2.4 Co-transfection of FLAG-p27 clones with Wnt10b expression vector.
293T cells were transfected with expression vectors FLAG-p27 WT, Y74F, Y88F, and Y88F Y89F mutant clones (A) along with varying amounts of Wnt10b expression vector (0/1/2ug). Cells were lysed and analyzed by SDS-PAGE and Western Blot (B) to compare relative protein levels.

To determine whether these residues play a role in Wnt10b modulation of p27 protein turnover, plasmid vectors expressing N-terminal FLAG tagged p27 were site mutagenized to replace those Src-targeted tyrosine residues with alanines. These expression vectors for FLAG-p27 (1ug) were co-transfected into 293T cells along with Wnt10b expression vectors (0/1/2ug). Immunoblot analysis of cell lysates revealed that FLAG-p27 displayed a weak correlation with the quantity of WNT10B protein (Figure 2.4). However, this correlation was inconsistent in replicate experiments, which demonstrated significant deviation from Wnt10b expression and the expected p27 protein level (Figure 2.5).
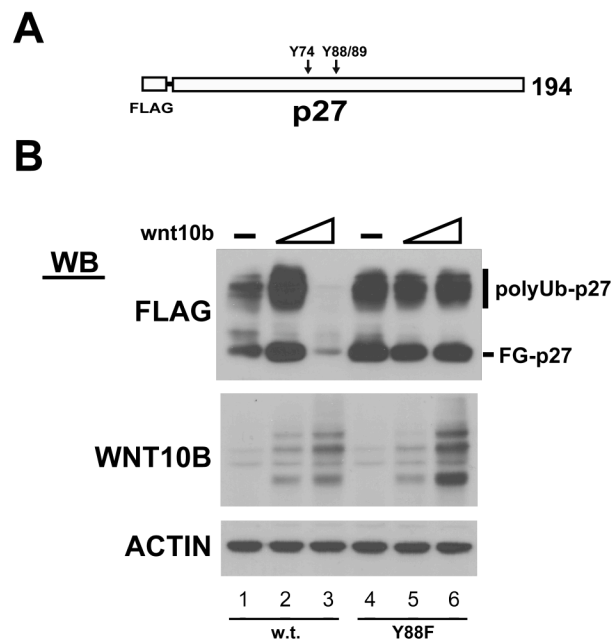
Figure 2.5 Co-transfection of FLAG-p27 clones with Wnt10b expression vector.
293T cells were transfected with expression vectors FLAG-p27 WT and Y88F mutant (A) along with varying amounts of wnt10b expression vector (0/1/2ug). Cells were lysed and analyzed by SDS-PAGE and Western Blot (B) to compare relative protein levels.

Furthermore, the assumption that the quantity of transfected expression vector correlated with the degree of protein expression failed to hold true despite great care taken in preparing the DNA for transfection. In figure 2, identical quantities of FLAG-p27wt were

transfected into 293T cells for wells 1-3 with increasing quantities of Wnt10b. While Wnt10b protein expression appeared to have a direct relationship with the amount of transfected expression vector, FLAG-p27 was highly variable. Our findings suggest that such an experimental strategy utilizing co-transfection is prone to generating inconsistent data.

Treatment of p27 transfected 293T cells with Wnt mimetics fail to impact p27 protein levels

Despite the weak and inconsistent correlation of p27 and Wnt10b protein expression, it was possible that the amount of Wnt10b vector used was insufficient. Previous experiments had used up to 5ug of Wnt10b vector alongside 1ug of FLAG-p27 in co-transfection experiments to show downregulation of p27 [70]. In addition, due to the inconsistencies in protein expression of when transiently transfecting different formulations of two separate expression vectors, an alternative method of activating the Wnt pathway was attempted through incubating cells with the Wnt mimetic SB216763 that acts via inhibition of GSK3 beta, a component of the "destruction complex" responsible for phosphorylating beta catenin and targeting it for turnover.
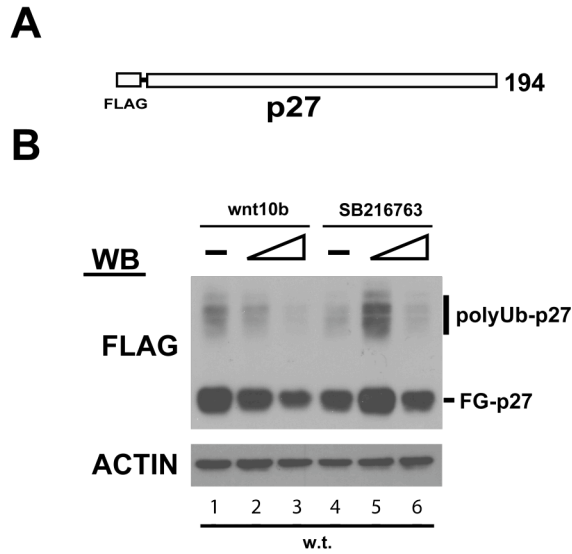
Figure 2.6 Co-transfection of FLAG-p27 clones with Wnt10b expression vector and treatment with SB216763 wnt mimetic.
293T cells were co-transfected with FLAG-p27 WT (A) and varying amounts of Wnt10b expression vector (0/1/2ug) or treated with SB216763 (0/6/12uM). Cells were lysed and analyzed by SDS-PAGE and Western Blot (B) to compare relative protein levels.

FLAG-p27 vectors were introduced into 293T cells through replicate transfections containing identical mixtures of p27 and Wnt10b plasmid DNA and treated with SB216763. While there appears to be a correlation between the quantity of p167 Wnt10b transfected and the expression level of FLAG-p27wt, the relationship was still not as significant as reported in previous experiments (Figure 2.6). On the other hand, there was no such relationship in SB216763 treated cells of identically transfected 293T cells. More troubling, the second transfected well that was treated with a low dose of SB compound had higher expression of FLAG-p27 than the other two corresponding wells. In addition to the SB216763 compound, we tested the Wnt mimetic LiCl, which also targets GSK3 beta. In duplicate experiments, FLAG-p27wt and T187A mutant were transfected into 293T cells and subsequently treated LiCl. The replicates gave dramatically differing results (Figure 2.7).

26
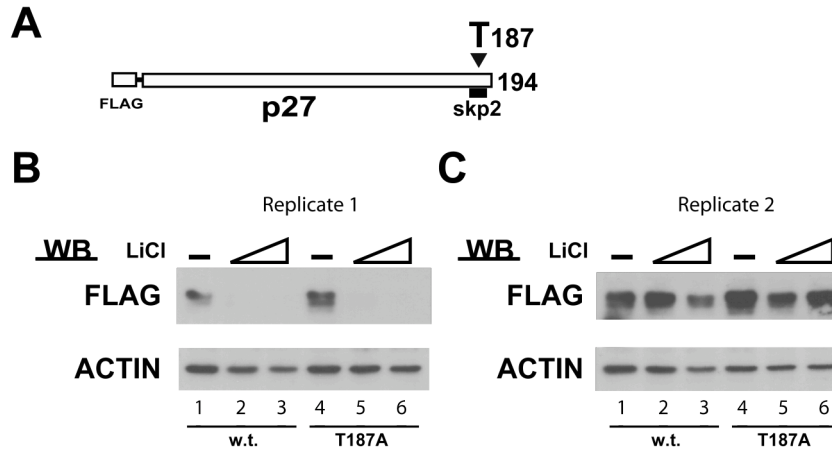
Figure 2.7 Co-transfection of FLAG-p27 clones with Wnt10b expression vector.
293T cells were transfected with (A) expression vectors FLAG-p27 WT and T187A mutant. Transfected cells were treated with Lithium Chloride (0/25/50uM) for 24h (B-C). Cells were lysed and analyzed by SDS-PAGE and Western Blot (B) to compare relative protein levels. The experiment was performed in duplicate to assay variation between replicates.

While replicate 1 had undetectable FLAG-p27 in both the LiCl treated samples, there was little effect in replicate 2. Given that the SB216763 and LiCl treated wells were transfected with identical conditions, this significant variation is cause for concern regarding the consistency and reproducibility of transient transfection experiments for measuring protein turnover even when separate transfections have identical formulations.

Real time PCR analysis of transiently transfected 293T cells

The fundamental assumption underlying the transient transfection experiments was that there was a direct correlation between the quantity of transfected plasmid DNA and the resulting protein expression. Based on the lack of reproducibility in our previous experiments, it was hypothesized that experimental variations in the relative amounts of co-transfected plasmid DNA had a non-linear effect on the efficiency of transfection and degree of transgene expression.
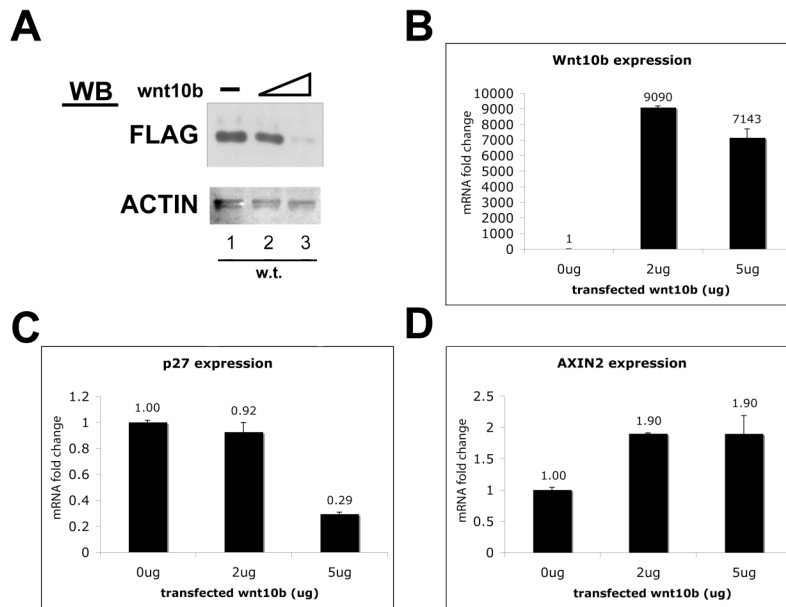
Figure 2.8 Real time PCR analysis of FLAG-p27 & Wnt10b co-transfection experiment. 293T cells were transfected with expression vectors FLAG-p27 WT along with varying amounts of Wnt10b expression vector (0/2/5ug). (A) Cells were lysed and analyzed by SDS-PAGE and Western Blot. Protein expression of p27 was compared to transcriptional activation of (B) Wnt10b, (C) p27, and (D) Axin2 to correlate mRNA expression with protein quantity.

In order to separate the post-translational protein turnover effect of Wnt10b signaling from methodological variations that impact mRNA expression, the transient co-transfection experiment was conducted but with an aliquot of cells analyzed by real time PCR for mRNA expression.

We found that while the highest amount of Wnt10b transfection correlated with a significantly lower amount of p27 protein, this effect was most likely due to differences in gene expression rather than proteasome turnover (Figure 2.8C). Although the amount of p27 plasmid (1ug) was kept constant between transfections, varying the amount of Wnt10b plasmid (0/2.5/5ug) was sufficient to effect substantial changes in both Wnt10b and p27 transgene expression. FLAG-p27 protein and mRNA expression were remained consistent when co-transfected with 0 and 2ug Wnt10b plasmid, but both were

28

dramatically lower in the 5ug Wnt10b co-transfected cells. FLAG-p27 mRNA expression and protein quanitites were tightly correlated to one another but not with Wnt10b mRNA expression. Wnt10b transfection coincided with a modest two-fold upregulation in Axin2 mRNA, but the degree of Axin2 expression did not correlate with p27 protein or mRNA levels. The evidence shows that the observed variation in FLAG-p27 protein level in the previous transient transfection experiments is likely due to variations in expression resulting from differences in transfection efficiency rather than from post-translational ubiquitin-proteasome mediated turnover.

Generated 293 T-REx stable cell line expressing tetracycline inducible p27

To get around the reproducibility issues of transient transfections, we decided to generate stable cell lines. Since expression of the cell cycle inhibitor p27 can cause G1 arrest, we opted for using the "T-Rex Tet On" system that allows for control of gene expression by addition of tetracycline. The 293 T-REx cell line constitutively expresses the Tet repressor protein, which exists as a homodimer and binds to the tandem Tet operator sequence located immediately downstream of the CMV promoter on the pcDNA5 FRT TO DEST expression vector into which the p27wt ORF was cloned. The vector also fused the p27 ORF with an N-terminal 3X-HA 3X-FLAG tag to facilitate affinity purification. Tet operator binding efficiently represses transcription, which is relieved by the addition of tetracycline that instigates a conformation change in the Tet repressor that renders it unable to bind the Tet operator.
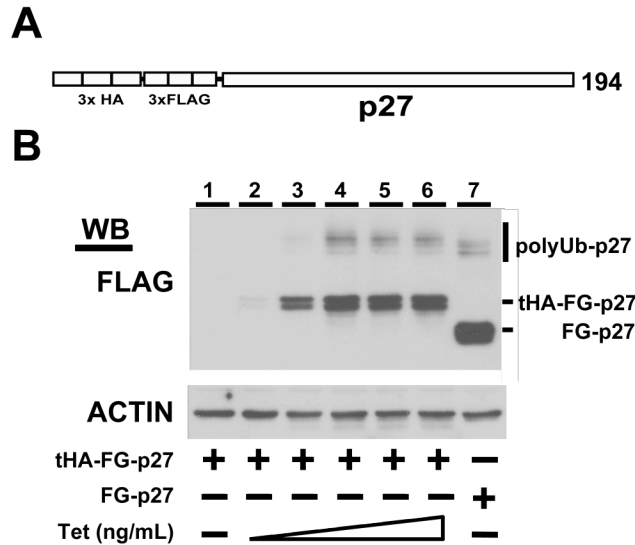
Figure 2.9 Tetracycline dose response for p27 in 293 T-REx cells.
293T-REx cells with tetracycline inducible expression p27 wild-type (A) were treated with varying concentrations of tetracycline (0/1/10/100/1000/2000) to induce 3HA-3FLAG-p27 expression (B). Cells were lysed and analyzed by SDS-PAGE and Western Blot (B). Included was a positive control cell extract expressing FLAG-p27 to show constitutive activation.

Additionally, the T-Rex system has the added benefit of allowing insertion of a single copy of the target gene into the host cell genome through recombination of the expression vector into a specific site. The sensitivity of protein expression in response to tetracycline treatment proved to be high with maximal p27 expression achieved within 100ng/mL tetracycline (Figure 2.9).

Real time PCR analysis of Wnt pathway induction in 293 T-REx cell line

To study the effect of Wnt signaling on p27, it is first necessary to establish that the cell line being used is Wnt responsive. While earlier experiments have been used to show Wnt modulation of p27 in HEK293T cells, the suitability of the 293 T-REx cellular background for investigating the Wnt pathway has not been demonstrated. Given that the transient transfection of Wnt10b may be responsible for producing spurious and misleading data, we sought to examine the effect of varying modalities for Wnt pathway activation.

Since Wnt responsiveness of a particular cell line depends initially upon the surface expression of Frizzled and LRP co-receptors, certain cell lines lacking the appropriate surface proteins may fail to activate the canonical Wnt pathway following addition of Wnt ligands. Other methods target the intracellular signal transduction pathway such as the GSK3 beta destruction complex, beta catenin, or downstream TCF/LEF transcription factors. The use of small molecule Wnt mimetics like lithium chloride bypasses the surface by diffusing through the cell membrane and targeting the GSK3 subunit of the destruction complex that resides in the cytoplasm [83]. However, the role of lithium as a Wnt mimetic may be complicated by its off-target effects [84].

A
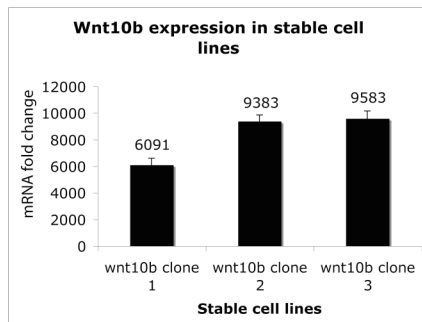
C
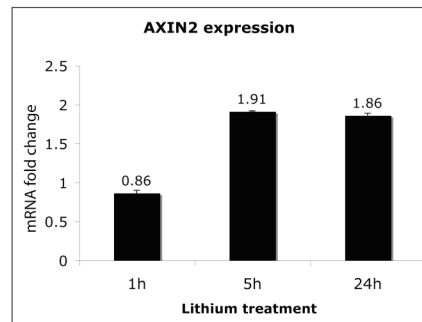
B
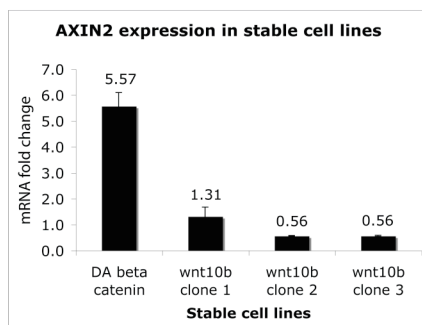
Figure 2.10 Real time PCR analysis of AXIN2 induction in HEK293 T-REx cells
293 T-REx cell lines were evaluated for mRNA expression of the Wnt target gene AXIN2 by real-time PCR. Three separate Wnt10b stable cell line clones were analyzed alongside a dominant active beta catenin stable cell line for (A) Wnt10b and (B) AXIN2 expression. (C) Lithium chloride treated 293 T-REx cells were also evaluated at 1/5/24h time points.

Wnt pathway activation was assayed by measuring the degree of AXIN2 mRNA upregulation. AXIN2 is a component of the GSK3 beta destruction complex that targets

beta catenin and is frequently upregulated by Wnt signaling as part of a negative feedback loop [85]. The real time PCR results show that stable Wnt10b expression has minimal and variable effect on AXIN2 transcription with one clone having slightly elevated expression in contrast to two clones experiencing a drop in expression. Lithium treatment caused a modest induction of AXIN2 mRNA by the 5h time point, which was sustained up to 24h. Dominant active beta catenin achieved the most significant upregulation of AXIN2 mRNA (Figure 2.10).

p27 wild-type and T187A mutant display similar turnover rate
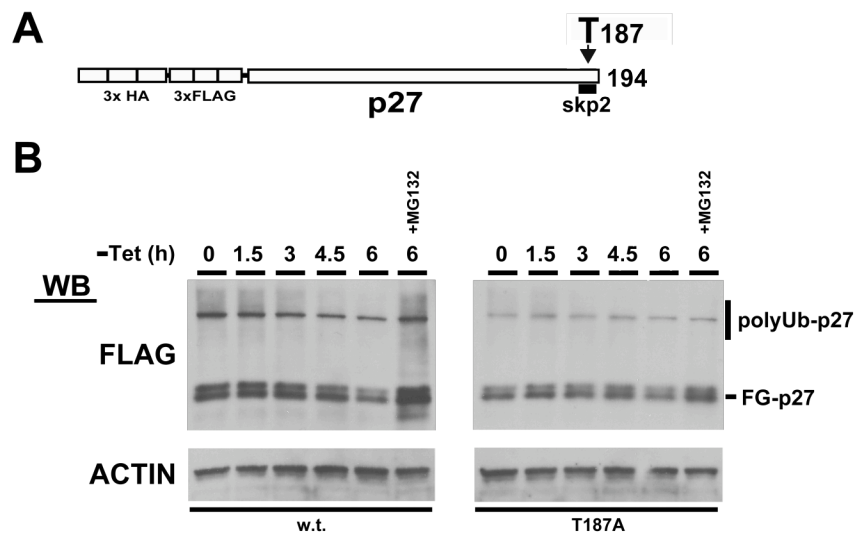
Figure 2.11 Wild-type and T187A mutant p27 turnover.
(A) 293 T-REx stable cell lines expressing tet-inducible wild-type and T187A mutant p27 were split into duplicate wells and then incubated with tetracycline (200ng/mL) overnight. (B) After 16h of tetracycline incubation, cells were washed in PBS to remove tetracycline and stop transcription of the transgene. The last well for each cell line was treated with 10uM MG132 after the PBS wash to inhibit proteasomal degradation. Cells were lysed and analyzed by SDS-PAGE and Western Blot.

Since Wnt signaling is presumed to catalyze p27 turnover within the context of multiple other pathways including SCF^{SKP2} modulated ubiquitylation, we wanted to eliminate the SKP2-dependent turnover by mutating the T187 residue to better focus on the Wnt-driven turnover. 293 T-REx stable cell lines for p27wt or T187A mutant were assayed for rate of

UPS-dependent protein turnover to determine the baseline rate of turnover. P27 expression was induced with tetracycline treatment overnight, followed by removal of the tet through PBS washes, after which cell lysates were collected at set time points (0/1.5/3/4.5/6h). The final time point was collected in duplicate with and without treatment with the proteasome inhibitor MG132. This strategy is essentially a pulse chase experiment because it induces maximal FLAG labeled p27 expression before abruptly ceasing further production. The data seemed to show a fairly similar rate of turnover for both wild-type and T187A mutant, which appeared noticeable by 6h when compared to the MG132 treated sample that had a significantly higher level of p27 (Figure 2.11).

This experiment was repeated but under treatment with 20mM NaCl or LiCl. The sodium served as a negative control to account for salt effects that can affect cells at higher concentrations. LiCl treatment failed to evoke a change in p27 protein turnover relative to NaCl controls (Figure 2.12).
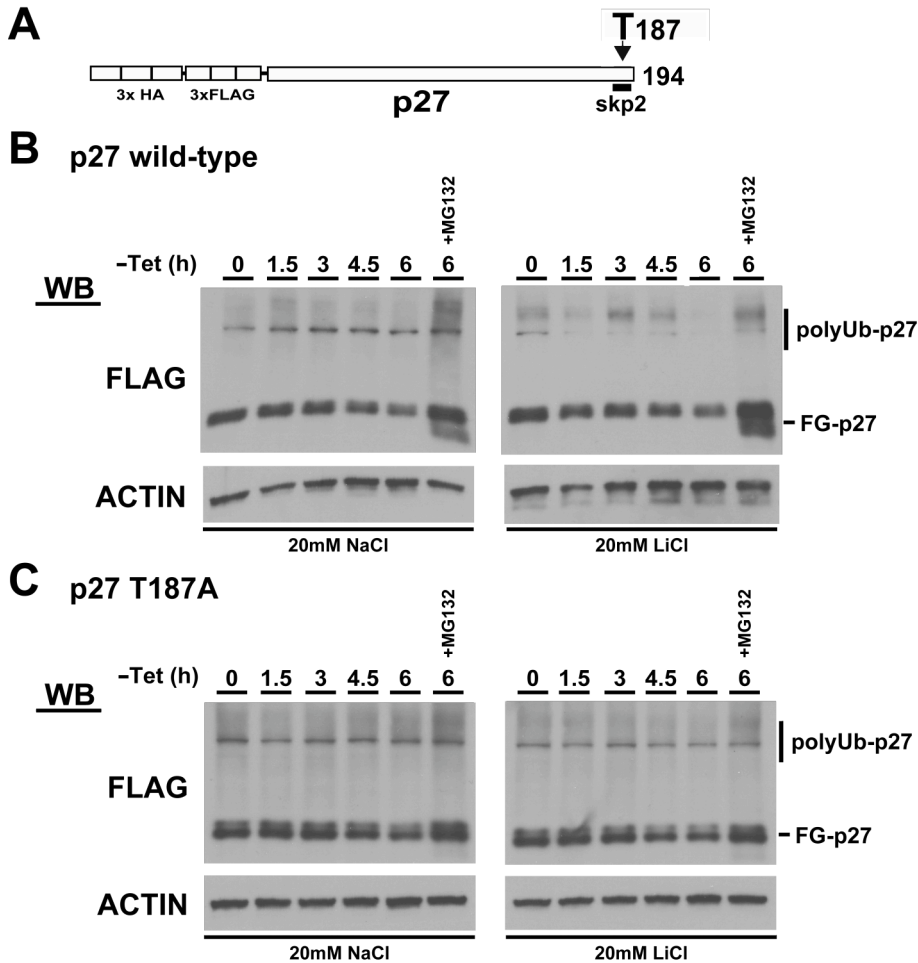
Figure 2.12 Impact of lithium on wild-type and T187A mutant p27 turnover.
(A) 293 T-REx stable cell lines expressing tet-inducible wild-type and T187A mutant p27 were split into duplicate wells and incubated with tetracycline (200ng/mL) and LiCl (B) or NaCl (C) (20mM) for 16h. Cells were then washed in PBS, given fresh media containing LiCl/NaCl and then harvested at the indicated time points. The last well for each cell line was treated with 10uM MG132 after the PBS wash to inhibit proteasomal degradation.

p27 turnover in Wnt10b or dominant active beta catenin stable cell lines

The use of Wnt mimetics is complicated by their potential to have off-target effects. For example, lithium is known to inhibit both GSK3 alpha and beta, cyclo-oxygenase (COX), Akt, and inositol monophosphatases [83]. The unintentional inhibition of these enzymes could have confounded attempts to isolate the impact of Wnt signaling on p27 turnover. Therefore, we attempted a strategy of generating double stable 293 T-REx cell lines that express tet inducible p27 within the background of Wnt10b overexpression. Because 293

T-REx cells were not known to respond to Wnt10b ligand, we also chose to use dominant active beta catenin to activate the canonical Wnt pathway. Accordingly, two double stable cell lines were made with Wnt10b and dominant active beta catenin using the 293 T-REx p27 T187A stable cell line.
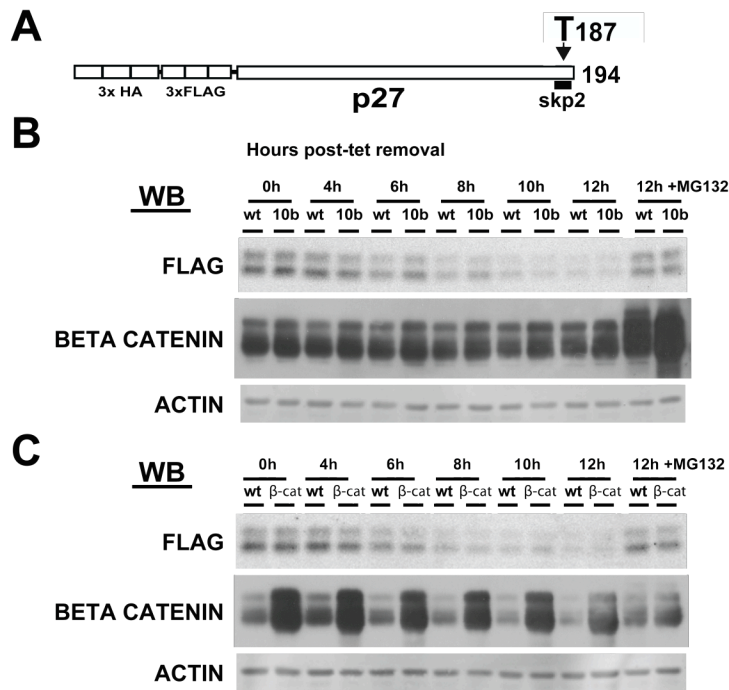
Figure 2.13 Mutant p27 T187A turnover in Wnt10b and dominant active beta catenin stable cell lines.
(A) 293 T-REx cells stably expressing tet-inducible wild-type and T187A mutant p27 and control, Wnt10b (B), or dominant active beta catenin (C) were split into duplicate wells and then incubated with tetracycline (200ng/mL) overnight. After 16h of tetracycline incubation, cells were washed in PBS to remove tetracycline and stop transcription of the transgene. The last well for each cell line was treated with 10uM MG132 after the PBS wash to inhibit proteasomal degradation. Cells were lysed and analyzed by SDS-PAGE and Western Blot.

We observed the rate of p27 T187A turnover by removing tetracycline and then harvesting them at set time points (Figure 2.13). While dominant active beta catenin was easily detected through Western Blots showing the enriched beta catenin present in the stable cell line, expression of Wnt10b did not appear to stabilize beta catenin to a degree that was observable compared to the negative control. In both cases, however, no differences were observed in the rate of p27 turnover.

SFB-DDB1 and p27 fail to co-purify

We sought to verify association of the CRL4 complex with p27 by co-immunoprecipitation. We obtained the expression vector for DCAF-binding protein DDB1, which was expressed with an N-terminal triple tag consisting of S tag, FLAG tag, and a streptavidin binding tag (SFB). This construct used to generate double stable 293 T-REx cell lines constitutively expressing the SFB-DDB1 along with tetracycline inducible 3HA-3FLAG-p27. Immunoprecipitation of SFB-DDB1 was carried out by incubation with streptavidin-conjugated sepharose beads followed by Western Blot for 3HA-3FLAG-p27.
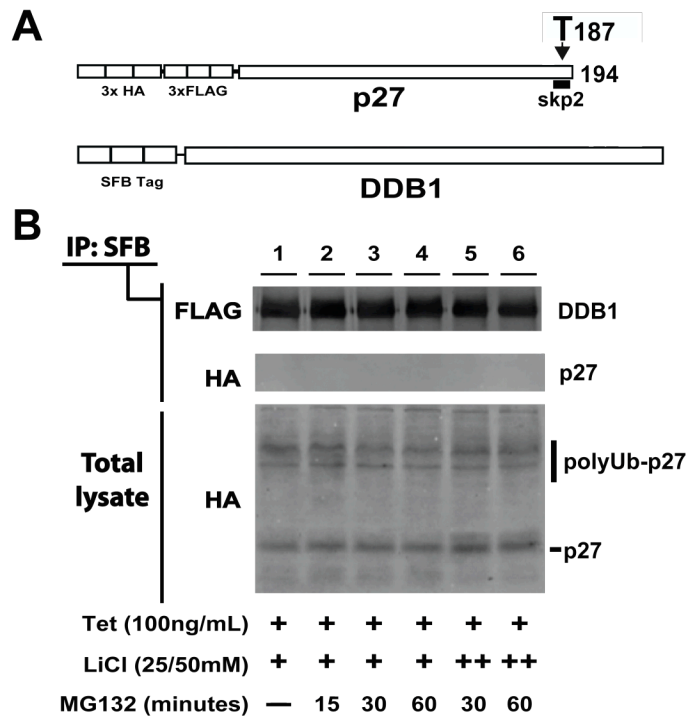
Figure 2.14 Analysis of SFB-DDB1 and 3HA-3FL-p27 binding by affinity purification.
(A) HEK293 T-REx SFB-DDB1 stable cell line was transfected with 3HA-3FLAG-p27 tet-inducible vector. (B) 24h post-transfection, cells were treated with tetracycline and lithium chloride 24h to induce 3HA-3FLAG-p27 expression and to induce Wnt signaling. Cells were incubated with the proteasome inhibitor MG132 (10uM) prior to cell lysis for the indicated durations. SFB-DDB1 was affinity purified from the total lysate with streptavidin-conjugated sepharose beads and eluted with biotin elution buffer. Samples were analyzed by SDS-PAGE and Western Blot.

As shown in Figure 2.14, purified SFB-DDB1 failed to co-precipitate p27. This result is not altogether unexpected. Due to the transient and processive nature of E3 ligase-substrate interactions, it can be difficult to purify a stable complex. Therefore, it is entirely possible that weak associations can still be detectable when conducted on a larger scale with greater quantities of protein lysate and using batch purification.

Analyze purified p27 by Mudpit MS/MS

We chose to screen for p27 associated proteins through tandem mass spectrometry analysis of batch purified 3HA-3FLAG-p27. Tagged p27 was expressed through tetracycline induction in the 293 T-REx pcDNA5 FRT TO DEST p27 stable cell line. Cell lysate was column purified with anti-HA sepharose beads and eluted in buffer containing dissolved HA peptide. Silver staining of purification fractions showed the successful
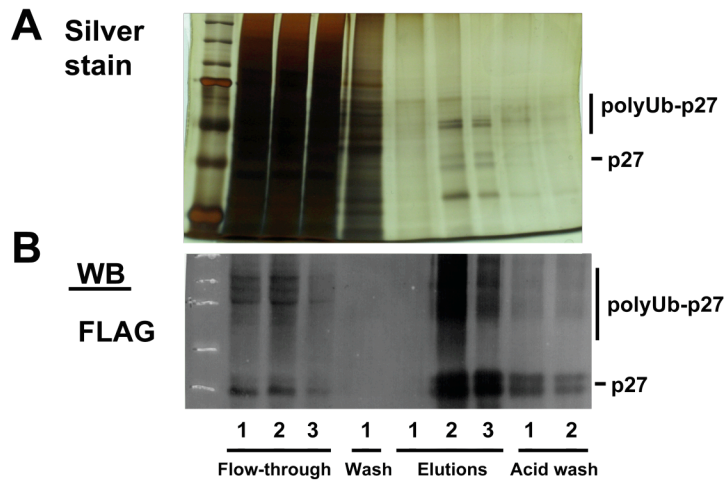
Figure 2.15 Silver staining and Western Blot of batch purified 3HA-3FLAG-p27
293 T-REx stable cell lines expressing tet-inducible p27 were incubated with tetracycline (100ng/mL) 16h. Cells were lysed and column purified with an anti-HA column. Representative samples from the flow-through, wash, elution, and acid washed fractions were resolved by SDS-PAGE. Purification of p27 was visualized by (A) silver staining and (B) Western Blot.

purification of p27 protein in sufficient quantities for Mudpit mass spectrometry analysis (Figure 2.15). Western Blot confirmed the specificity of the p27 elution sample. The eluted sample was prepared and analyzed by MS-MS.

Figure 2.16A displays the list of p27 associated proteins with a NSAF score greater than 100. The known and relevant p27 interactions were culled from this list to generate an interaction diagram, which includes cyclin dependent kinases 2/4/5 and various associated cyclins (Figure 2.16B).

A

Gene	Spectra	NSAF
CDK2	246	9510
CDKN1B	109	6342
CCNB1	172	4576
HSPA1L	196	3522
GPX4	54	3390
DSTN	38	2653
PRDX4	46	1955
CDK5	41.5	1732
PRMT1	52	1710
HPSA9	94	1594
CCNE1	54	1517
CCNA2	49	1306
PAICS	47	1263
PRDX3	27	1215
TUBB2C	39	1009
CDK4	26	988
TUBB	37	979
GRPEL2	18	921
SKP1	13	918
CCNB2	27	781
SSBP1	10	778
CBR4	14	775
CCND2	19	757
CKS2	5	729
Calnexin	16	677
HSD17B8	15	662
C21orf45	13	642
CCND1	13	507
EEF1AL3	18	448
NT5DC2	19	435
EEF2	32	429
DNPEP	18	427
PCBP1	13	420
BUB3	9	389
NEK9	33	388
CARM1	20	386
ISCU	5	372
PRMT5	20	366
TK1	7	344
CCND3	8	315
LANCL2	11	281
TUBA1	11	281
KIF11	24	261
DUT	5	258
EIF6	5	235
PFTK1/2	8	229
FBXO22	8	228
KHSRP	13	210
PPP2R2A	7	180
TRIM65	8	178
ZC3HC1	7	164
PEG10	7	156
GSTM3	3	153
RPIA	4	148
LANCL1	5	144
SDHA	8	138
STRAP	4	131
PPA1	3	119
MTHFD1	9	110
CPOX	4	101

B

Figure 2.16 MudPit mass spectrometry analysis of purified p27.
3HA-3FLAG-p27wt was purified by anti-HA immunoprecipitation and analyzed by tandem mass spectromy. Nonspecific interactions found in the negative control were removed along with NSAF scores below 100 (A). Identified proteins with known associations with p27 and E3 ligase subunits are displayed in interaction map (B). Direct lines connecting p27 to interactors are indicative of mass spectrometry data demonstrating their co-purification. Lines connecting interactors to each other are reflective of known binding partners based on the literature.

Our findings are corroborated by the extensive literature on p27 and its regulation of cyclin dependent kinase activity. P27 stably binds to Cdk2-cyclin A/E complexes and suppresses their kinase activity during G1. Cdk4-cyclin D complexes are regulated in a similar manner; furthermore, the presence of T157 and T198 phosphorylated p27 is critical to their stable assembly [86]. In both cases, p27 inhibited the Cdk/cyclin-dependent phosphorylation of retinoblastoma protein, which is necessary for the G1/S phase transition. Thus, the 3X HA-FLAG tagged p27 construct participated in relevant biological interactions with known partners.

Mudpit mass spectrometry also identified three SCF related components: CKS2, SKP1 and FBXO22. CKS2 and its relative CKS1 have important roles in modulating p27 stability. CKS1 is a co-adaptor in the SCF^{SKP2} complex and utilizes a phosphate recognition site to bind T187 phosphorylated p27 and target it for ubiquitylation [87]. CKS2 appears to have the opposite function and counteracts CKS1 by protecting p27 from ubiquitylation and proteasomal turnover [88]. SKP1 is a core subunit of the SCF complex, and is responsible for recruiting F-box proteins that target specific substrates. FBXO22 was an uncharacterized F-box protein that has recently been implicated in the ubiquitin-mediated proteasomal turnover of histone demethylase KMD4A and sarcomeric proteins [89, 90]. Notably missing from this list, however, are subunits of the CRL4 or any other E3 ligase complex.

2.5 Discussion

Transient transfection methods for studying protein turnover

We first sought to establish an experimental system that could faithfully reproduce the Wnt-induced effect of p27 turnover vis-à-vis the ubiquitin proteasome system. While the

technique of using co-transfection methods have been used to elucidate biomolecular pathways before, it is generally used to measure more direct functional relationships such as promoter activation with luciferase reporter constructs [91-93]. Conversely, co-transfection of Wnt10b and p27 expression vectors relies upon multiple assumptions to achieve an experimentally measurable effect.

First, the quantity of Wnt10b plasmid transfected is assumed to correlate linearly with the level of mRNA and protein expression. The Wnt10b protein is then presumed to be secreted and to effect paracrine signaling on neighboring cells. Wnt pathway activation itself depends upon the 293T/T-Rex cell line being responsive to this specific Wnt ligand, which necessitates expression of the appropriate Frizzled and LRP co-receptors. The intracellular signaling machinery must then inhibit the GSK3 beta destruction complex to prevent the targeting of beta catenin for proteasomal turnover. This leads to stabilization and nuclear translocation of beta catenin to activate transcription of Wnt target genes that presumably include components of the CRL4, including DCAF4s that confer p27 substrate specificity to the core complex. These downstream pathways may include other post-translational modifications of p27 such as phosphorylation that can mark it for polyubiquitylation. The UPS targeting and activation must also be sufficiently powerful to have an experimentally observable impact on the level of steady-state p27 protein that is constitutively expressed under the CMV promoter. The nature of transfection means that it is likely each transfected cell has endocytosed numerous copies of the expression vector with the effect that p27 expression is maximized. Against this molecular context, enhanced p27 turnover may be difficult to detect. These considerations may explain in large part why the immunoblots of

transiently transfected 293 T-REx cells failed to reproduce expected findings. The inherent variability of such an experimental system proves to be challenging for arriving at robust conclusions. For these reasons, we chose to move onto alternate strategies.

p27 analysis with stable cell lines

To avoid the inconsistencies of transient transfection, we decided to generate stable cell lines. Because p27 functions as a cell cycle inhibitor, constitutive expression could cause cell arrest in the putative stable cell line. This obstacle was avoided through the use of the 293 T-REx Gateway system (Invitrogen), which allowed for the controlled induction of p27 expression with tetracycline. While we sought to minimize SKP2-mediated polyubiquitylation of p27 by using T187A mutant p27 that cannot be phosphorylated and targeted to the SCF^{SKP2} E3 ligase, our time course experiments examining p27 turnover failed to establish any significant differences between mutant and wild type. Although studies have shown that mutating the T187 residue to prevent phosphorylation and polyubiquitylation by SCF^{SKP2} can counteracts p27 turnover, SKP2 has also been found to drive p27 proteolysis in a T187 phosphorylation independent manner in G1 [76]. In addition, the KPC1 ubiquitin ligase complex has been identified as an alternative pathway for degradation of p27 in G1 phase [94]. Therefore, one explanation for the lack of stabilization of p27 T187A protein is that pathway redundancies compensate for the loss of phospho-T187 dependent p27 turnover.

Inhibition of GSK3 beta with lithium also had no observable impact on the rate of turnover. While it is entirely possible that off-target effects could have confounded the results, time courses using double stable cell lines expressing Wnt10b or dominant active beta catenin reproduced this lack of enhanced p27 degradation. Given that the dominant

41

active beta catenin HEK293 T-REx stable cell line had a measurable upregulation of the Wnt target gene AXIN2, this finding cannot be attributed to a failure to activate the canonical Wnt signaling pathway. An alternate explanation is that the E3 ubiquitin ligase responsible for turning over p27 is already activated in the HEK293 T-REx cellular background used in our experiments. Since HEK293 cells are immortalized and are characterized by polyploidy and other genetic abnormalities, it is entirely possible that pathway mutations, which would have been necessary to overcome the inhibitory function of p27 on cell proliferation, happened to include activating mutations in our Wnt-driven E3 ligase pathway.

DDB1-p27 purification

This possibility led us to proceed with purifying p27 and characterizing its associated proteins in the search for E3 ligase components. Stable cell lines expressing core subunits of the CRL4 in addition to p27 were used in an attempt to isolate them in complex. Although the co-immunoprecipitation results did not provide strong evidence for physical interaction between them, it was not surprising that the transient nature of such an enzymatic association would be technically challenging to detect. Furthermore, the background evidence for a Wnt-driven ubiquitin pathway for p27 turnover was more compelling than the data specifying the CRL4 complex. This consideration carried the possibility that another E3 ligase instead of CRL4 could be behind the mechanism of SKP2-independent p27 turnover. Therefore, we decided both to increase the scale of our purification methods and to screen for E3 ligase components in an impartial manner through analysis of affinity purified p27 and its associated proteins using tandem mass spectrometry.

MudPit mass spectrometry data set for p27

MudPit mass spectrometry analysis identified a number of cyclins and cyclin dependent kinases that are consistent with the existing literature on known p27 interactions. P27 has been shown to physically bind and inhibit the activity of cdk2, cdk4, and cdk5 complexes. These findings provide encouraging validation that the N-terminal 3HA-3FLAG tag on the p27 construct does not inhibit functional interactions with binding partners. The dataset also included SCF-associated proteins SKP1, CKS2, and FBXO22. While SKP1 and CKS2 have been implicated in p27 targeting by SCF^{SKP2}, FBXO22 was a relatively unknown F-box protein presumed to be involved with the SCF complex and contained a C-terminal FIST domain that is frequently found on F-box proteins associated with the ubiquitin proteasome system [95]. Recently, FBXO22 was discovered to have a functional role in the ubiquitin proteasome system when it was discovered to catalyze the ubiquitylation of the histone demethylase KDM4A [89]. This potential link between FBXO22 and p27 can be explored in future research.

An unexpected result was the absence of SKP2, which was anticipated to be the highest scoring E3 ligase component given its key role in regulating p27. Furthermore, subunits from non-SCF E3 ligases were noticeably absent from the dataset. Besides the technical hurdles of attempting to purify transient ligase-substrate interactions, these findings raise additional biological considerations that complicate the goals of our screen. Specifically, there may be additional substrate recruiting factors that are necessary for association between p27 and the E3 ligase we seek to identify. For example, p27 turnover by the SCF^{SKP2} complex requires the presence of CKS1, and both p21 and DNA licensing factor Cdt1 are targeted by the CRL4^{Cdt2} ligase only with proliferating cell nuclear

antigen (PCNA) bound to their "PIP degron" [96, 97]. If Wnt-induced p27 targeting requires the additional presence of such factor(s), then the cellular context utilized for such in vitro experiments will have to be completely re-evaluated to find both an appropriate cell line and the right method of activating Wnt signaling. Simply put, the preponderance of the empirical evidence argues that there is no Wnt modulated pathway that targets p27 for ubiquitin-proteasome dependent proteolysis in HEK293 T-REx cells in a SKP2-independent manner.

CHAPTER 3 Elucidation of the Wnt modulated CRL4 substrate adaptor DCAF4

3.1 Background

Wnts comprise a highly conserved family of secreted growth factors that has been implicated in a variety of developmental processes including body patterning and tissue differentiation [17, 98]. Wnts have also been shown to play a role in tissue specific stem cell maintenance, and there is evidence suggesting the involvement of Wnt signaling in mammary stem cell tumorigenesis [16]. A growing body of evidence has linked aberrant Wnt signaling to various cancers such as the colorectal cancer familial adenomatous polyposis which results from inherited, inactivating mutations to the adenomatous polyposis coli (APC) component of the destruction complex that targets beta catenin for degradation [99-103]. We have previously shown that the mammary specific Wnt10b is capable of targeting the cell cycle inhibitor p27^{kip1} for proteasomal turnover via the CUL4 DDB1 E3 ligase [70]. Our finding built a foundation for investigating the interaction between Wnt signaling and the ubiquitin proteasome system. Consequently, we sought to identify E3 ligase components that were transcriptionally modulated as Wnt target genes. Of particular interest were the E3 ligase substrate adaptors that conferred binding specificity.

E3 ligases utilize a wide array of adaptors that recruit substrates to the ubiquitylation machinery. Substrate targeting is elucidated by the molecular architecture of E3 ligases, which center on a rigid scaffolding component. This central backbone recruits additional subunits that confer functionality and specificity. For example, the well-characterized SCF complex is organized around the scaffolding component CUL1. Comprised of a globular domain that recruits RBX1 through a beta sheet interaction

surface and a long alpha helical domain that binds the SKP1-F-box protein module, CUL1 acts to organize the E2-ubiquitin and substrate recruiting subunits for optimal positioning of ubiquitylation substrates [104]. More recently, the crystal structure of the CUL4 DDB1 E3 ligase showed remarkable organizational similarities to the SCF complex with a CUL4 scaffolding component that recruits RBX1 and DDB1, which appears to fulfill an analogous substrate adaptor role to SKP1 [105, 106].
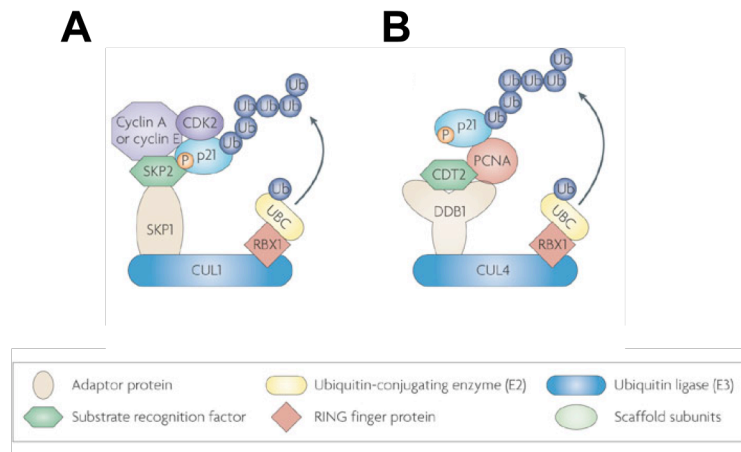
Adapted from Abbas et al 2009 (Ref)

Figure 3.1 Comparison of SCF and CRL4 complexes.
This figure illustrates the analogous functions of the (A) SCF and (B) CRL4 E3 ligase complexes. Both utilize a central Cullin scaffolding module that binds on one end to a RING finger protein which recruits the E2 ubiquitin conjugating enzyme. The other end binds to the substrate binding components including the adaptor and substrate recognition factors.

These similarities are illustrated in Figure 3.1, which shows both complexes utilizing their unique components in analogous positions to target the same p21 substrate [107]. The relatively recent advent of mass spectrometry has allowed for groundbreaking research on the identification of purified components of the CRL4 complex, which yielded the identities of dozens of DCAFs [106, 108]. Specific DCAFs have been implicated in a variety of functions including the targeted ubiquitylation of substrates such as the DNA licensing factor Cdt1 and the cell cycle inhibitor p21, and DNA methylation [109-111].

The Waterman lab shared data from a microarray screen that suggested Wnt modulation of four WD40 genes: WDR3, WDR21A, WDR33, WDR71 (comm. Dr. Waterman, UCSD). They conducted their screen in a DLD1 colorectal cancer cell line with constitutive activation of the Wnt pathway due to APC-inactivating mutations. Within this background active Wnt signaling, they had modified the cell line to stably express a tetracycline regulated dominant negative TCF1 "E form" transcription factor [112]. Expression of the downstream Wnt activator TCF1 in its dominant negative "E form" results in competitive inhibition against the activities of endogenous TCF1, and thus affects the expression of Wnt target genes [112]. We identified WDR21A as the CRL4 adaptor DCAF4 and confirmed its transcriptional modulation by Wnt signaling, and present the results of our investigation into its structure and function.

Project Aims

A) Validate modulation of WD40 gene expression by Wnt signaling.

B) Determine whether WD40 genes are DDB1 and CUL4 Associated Factors (DCAFs).

C) Investigate functions and target substrates of validated DCAFs.

3.2 Materials and Methods

***All vectors and oligos are listed in Appendix Table A.1**

Plasmid Vectors & Modification

The pCMV6-Entry vectors for WDR3, WDR33, WDR71, WDR21A isoforms 1 and 2 were obtained from Origene Technologies. We modified the Entry vectors for WDR21A to incorporate a 2X Tet^R operator sequence immediately downstream of the CMV promoter to allow control of transcription by the addition of tetracycline. The Tet^R operator sequence was designed from the 2X Tet Operator located within the pcDNA5

47

FRT TO DEST vector (Invitrogen). The determination was made to insert the Tet Operator using a Sac I restriction site located at an optimal position immediately downstream of the CMV promoter and TATA box and upstream of the transcription initiation site. The operator sequence was designed as an oligonucleotide pair flanked by the Sac I restriction site. An additional Afl II restriction site was included to serve as a marker for successful insertion of the Tet^R operator within the target vector. The oligonucleotide pair was ordered from MWG Operon with 5' phosphorylated ends, which are required for successful T4 ligase-mediated DNA ligation. The lyophilized forward primer and reverse primers were reconstituted in ddH$_2$O at 100uM. Primer aliquots were combined in a 1:1 ratio for a final concentration of 50uM and then mixed with 1X T4 ligase buffer. This oligo solution was annealed to form the Tet^R operator by heating to 95C and then slowly cooling to room temperature on a PTC thermocycler (MJ Research). The pCMV6-Entry vectors were restriction digested with Sac I (NEB) enzyme at 37oC for 1h and then heat inactivated by incubating at 80°C for 5min. The linear vectors were then CIP treated for 1h at 37C to remove the phospho groups on the 5' and 3' ends, which is necessary to prevent vector self-ligation. The digests were then gel purified using a gel purification kit to isolate the linearized vectors and to remove enzymes and buffer components that could interfere with ligation (Qiagen). The annealed Tet^R Operator and linearized pCMV6-Entry vectors were then ligated at a 3:1 ratio with T4 DNA ligase at 16°C overnight (NEB). T4 DNA ligase was heat inactivated by incubating at 65°C for 10 minutes, and aliquots of the ligations were transformed into RapidTrans TAM1 competent cells (Active Motif). Plasmids were confirmed by restriction digestion

with the Afl II site located in the Tet^R Operator and by sequencing with CMVf and T7 primers.

N-terminal EYFP fusion

Using cloning techniques described above, the pCMV6-Entry DCAF4 ORFs were fused with EYFP at the N-terminus to allow visualization of DCAF4 in live cell cultures. The EYFP fusion protein was amplified from pcDNA3.1 EYFP vector with primers that flanked the EYFP ORF with SgfI restriction sites: This allowed the PCR product to be digested by SgfI and then inserted just upstream of the transcription start codon on the SgfI digested pCMV6-Entry DCAF4 vector to generate N-terminal EYFP fusion. Ligation clones were validated by sequencing and visualization of fluorescence in transiently transfected 293 T-REx cells.

DCAF4 deletion mutations

Deletion mutagenesis of the N-terminal domain located within the ORF of pCMV6-Entry DCAF4 isoform 1 vectors was carried out using the mutagenesis protocol described above. However, due to the decreased energy favorability of primer-template binding in deletion mutagenesis compared with site mutagenesis, the primer pairs were then further modified to reduce the complementarity overlap in order to enhance primer-template hybridization [113]. This method using mismatched primer pairs proved to have a superior rate of success compared to the previous method that utilized primer pairs with 100% matching identity. Clones were first analyzed by restriction digests and DNA sequencing, and then validated through Western Blot of expressed DCAF4 protein. Deletion mutagenesis was also used to generate DCAF4 isoform 3 from isoform 1 via PCR-mediated truncation mutation that excised exons 5 and 6.

Site-directed PCR mutagenesis

Mutagenesis primers were initially designed to mutate the WDxR motif located at 297-300 amino acid residues within one of three DCAF4 WD40 domains using the techniques described above. PCR mutagenesis of pCMV6-Entry DCAF4 wild-type vectors was carried out using high fidelity Deep Vent polymerase (NEB) for 16 cycles of 1min 95°C denaturation, 1min 60°C annealing, and 10min 72°C extension. The original template vector was eliminated with Dpn I digestion at 37°C for 2h. DNA precipitation was carried out by addition of 1X volume of 100% ethanol and 2uL of glycogen, followed by incubation at -20°C for 30min. Precipitated DNA was pelleted by centrifugation, washed once with 70% ethanol, air dried, and dissolved in TE buffer. Aliquots were transformed and plated using TAM1 competent cells. Clones were validated by DNA sequencing.

General maintenance

293TREx, HeLa TREx, MCF7, and MCF15 cells were grown in high glucose DMEM supplemented with 10% Fetal Bovine Serum, 2mM L-glutamine and penicillin/streptomycin (Omega). DLD1 cells were grown in RPMI 1640 supplemented with 10% Fetal Bovine Serum, 2mM L-glutamine and penicillin/streptomycin. Cells were maintained at 5% CO_2 in 37°C incubators. Cells were passaged by washing once with PBS, incubating with trypsin for 5min at 37°C 5% CO_2, neutralizing with 3mL complete media, pipet mixing, then centrifuging at 500rpm for 5min, aspirating supernatant, and finally plating in a new dish. Cell culture additives lithium and sodium chloride, cycloheximide, MG132, and tetracycline were all prepared as described in chapter 2.2 methods & materials.

Like the HEK293 T-REx cell line, HeLa T-Rex cells stably express the Tet repressor protein, which binds to a recognition Tet operator sequence to suppress downstream gene expression in the absence of tetracycline. DCAF4 stable cell lines were generated by transfecting linear pCMV6-TetO-DCAF4 vectors into HEK293 T-Rex cells by calcium phosphate. Two days following transfection, cells were selected with G418 1mg/mL for 2 weeks before colonies were picked and assayed for tetracycline-induced expression by Western Blot or fluorescence microscopy in the case of EYFP-fusion proteins. Tetracycline was used at 200ng/mL final concentration for inducing gene expression. MCF15 cells were transfected with superfect transfection reagent (Qiagen).

Real time PCR

RNA was extracted using the Qiagen Rneasy plus mini kit. First strand cDNA synthesis was carried out using 1ug RNA with reverse transcriptase and random primers with a 2h 37°C incubation followed by a 10min 95°C heat inactivation step (Applied Biosystems Superscript cDNA kit). PCR reactions were performed using 1X SYBR Green master mix (Veriquest PCR SYBR Green Master MIx) with 0.3uM primer concentration on a real time PCR machine (Stratagene MX3000P Real-Time PCR system). Cycling conditions were as follows: 10min 95°C initial denaturation, 40 cycles of 15s 95°C denaturation, 15s 60°C annealing, and 30s 72°C extension. Real time PCR primers were designed using the NCBI primer blast site.

at 10uM to minimize proteasome-dependent protein turnover.

DCAF4 protein dephosphorylation

293 T-REx DCAF4 stable cells treated with tetracycline overnight were split into two aliquots and lysed in the EBC lysis buffer with and without phosphatase inhibitors added.

The extracts without phosphatase inhibitor were then incubated at 37°C 30min with CIP. Samples were analyzed by SDS-PAGE and Western Blot.

Cell extraction and Immuno-blotting

Cells were lysed in a mild, nonionic buffer (100mM Tris, 150mM NaCl, pH 8.0 and 0.1% Nonidet P-40) supplemented with protease and phosphatase inhibitors (Complete™ Mini and PhoSTOP; Roche Applied Science) for 30min on ice. The samples were pelleted at 14,000 RPM for 15 min, 4°C. Protein concentrations were determined using the BioRad Protein Assay (BioRad Labs, Hercules CA). For analysis by immunoblot, protein samples were separated by SDS-PAGE gels. Separated proteins were then transferred onto PVDF-Q^{FL} membranes at 22V overnight (Immobilon). Membranes were blocked with Odyssey blocking buffer for 1h at room temperature and then incubated with primary antibodies in Odyssey blocking buffer overnight at 4°C, washed 3X in PBST, and blocked with secondary antibodies in Odyssey blocking buffer 0.1% Tween20 0.01% SDS for 1h at room temperature. Following three final washes in PBST, the membranes were scanned with a LiCor Odyssey imager.

Immunoprecipitation

FLAG-tagged protein lysates were pre-cleared by incubating with GST-sepharose beads for 1h at 4°C while inverting gently. The supernatant was then incubated with anti-FLAG M2 EZView beads (Sigma) overnight at 4°C. Following three washes in IP wash buffer (150mM NaCl 50mM Tris pH 8.0, protease inhibitors), the beads were eluted for 15 minutes at room temperature using FLAG tripeptide elution buffer (FLAG tripeptide dissolved in EBC lysis buffer). The eluate was combined with 6X Laemmli buffer and boiled for analysis by SDS-PAGE and immunoblotting.

Immunofluorescence

Adherent HeLa TREx cells were grown in 8-well chamber slides (LabTek). Cells were fixed with 4% PFA for 10 minutes at room temperature, then washed with PBS. The slides were permeabilized and blocked with PBS containing 0.5% Tween20 and 1% BSA for 1h at 4°C. Slides were incubated with primary antibodies in blocking buffer overnight at 4°C in the dark. Following 3X PBS washes, the slides were incubated with secondary fluorescent antibodies (anti-rabbit/mouse Alexa fluor 488/633 from Invitrogen) in blocking buffer for 1h at room temperature. After three final PBS washes, slides were mounted with Vectashield supplemented with DAPI, and then visualized by fluorescence microscopy.

siRNA transfection

Lyophilized siGenome pooled siRNA against DCAF4, DDB1 and scrambled control were obtained and diluted in 1X siRNA buffer at 20uM stock concentrations (Thermo Scientific). Target cells were plated at 25% confluence 2h prior to siRNA transfection. Transfection was carried out using Superfect transfection reagent with siRNA at a final 20nM concentration (Qiagen). Cells were maintained for 2 days before they were analyzed.

MudPIT sample preparation and analysis

IP reactions and cell lysates were prepared the same as described above, but were scaled up in volume. Ice cold 100% TCA was added to IP elutions to a final 20% concentration and incubated overnight at -20C to precipitate the purified proteins. TCA precipitated proteins were pelleted by spinning at 14k rpm for 20min and washed 3X in ice-cold acetone. The pellets were air-dried, tryptically digested, and analyzed by MudPIT [114-

116]. The digested peptides were fractioned by a 4-step multidimensional chromatographic separation before MS-MS analysis by the LTQ-Orbitrap mass spectrometer (Thermo Fisher). Data analysis of the resulting peptide spectra were performed using SEQUEST and DTASelect algorithms [117, 118]. Identified proteins co-precipitating with DCAF4 isoforms were compared against negative control samples to screen out nonspecifically purified proteins. For the purposes of this study, the dataset was further analyzed against previously confirmed interactions with components of the DDB1-CUL4 E3 ligase. Further details on the workflow for proteomic analyses can be found elsewhere [119].

3.3 RESULTS

Wnt signaling modulates mRNA expression of a subset of WD40 genes

We obtained from the Waterman lab a clone of the DLD1 cell line expressing tetracycline inducible dominant negative TCF1E. Following tetracycline treatment for 24h, isolated mRNA was quantified by real time PCR analysis. Expression of the APC destruction complex component AXIN2, generally regarded as a global Wnt target gene and marker of Wnt activity, was found to be downregulated [85]. While WDR33 remained unaffected, TCF1E was found to repress WDR3, WDR21A, and WDR71, which suggest that these are Wnt target genes (Figure 3.1A).

In a separate experiment, we used the MCF15 cell line to assay the effect of Wnt pathway activation on the WD40 genes. This particular cell line was chosen because it was characterized as a basal mammary epithelial cell line [120]. Given the influence of the Wnt10b pathway on basal stem/progenitor mammary epithelial cells and mammary gland development, it was hypothesized that MCF15 cells would be Wnt responsive.
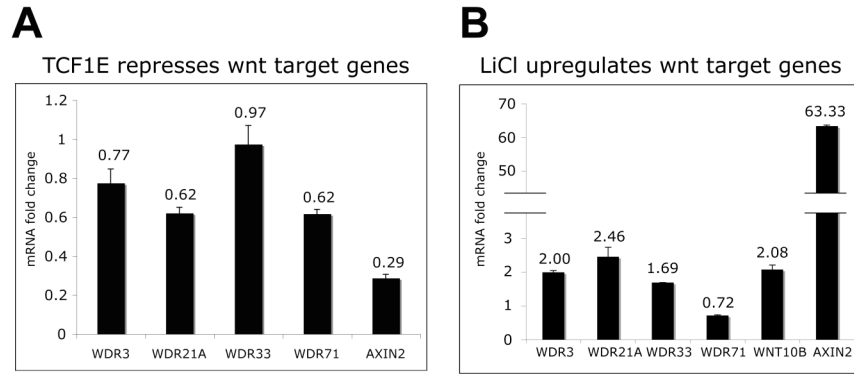
Figure 3.2 Wnt modulation of WD40 gene expression
(A) DLD1 cells expressing tetracycline inducible TCF1E were treated with 200ng/mL tet for 24h. Cells were then harvested for real time PCR analysis of WD40 gene expression. Wnt target gene AXIN2 was used as a positive control. (B) MCF15 mammary epithelial cells were treated with LiCl (20mM) for 6h. Cells were analyzed by real time PCR to determine extent of wnt driven WD40 gene upregulation. WNT10B and AXIN2 expression were analyzed as positive control wnt target genes.

This prediction was confirmed when MCF15 was found to be highly responsive to the GSK3beta inhibitor lithium chloride, which acts as a Wnt mimetic. Wnt responsiveness was demonstrated by the dramatic upregulation of AXIN2 mRNA following 6h incubation (Figure 3.1B). This was mirrored by a moderate increase in WDR3, WDR21A, and WDR33 expression with no change to WDR71.

WDR21A/DCAF4 successfully co-precipitates DDB1

The subset of WD40 genes that are known to interact with the CRL4 complex share a highly conserved WDxR/DxR motif that mediates binding between the WD40 beta propeller interaction surface with DDB1. Figure 3.3 shows the structure of the alternative splicing isoforms of WDR3, WDR21A/DCAF4, WDR33, and WDR71. While all of them have WD40 domains, only WDR3 and 21A have the DxR motif that characterizes typical CRL4 DCAFs.
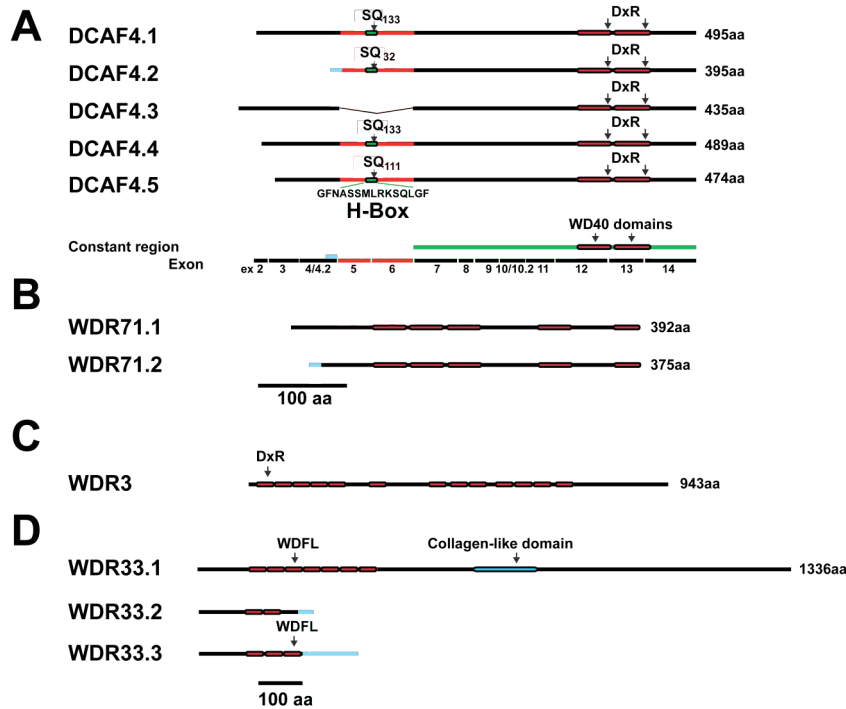
Figure 3.3 WD40 functional domains
WD40 genes are characterized by WD40 domains. CRL4 associated WD40 genes typically share a conserved DxR motif important for binding DDB1. (A) DCAF4 contains two WD40 domains with DxR motifs, while (C) WDR3 has a single DxR motif. (D) WDR33 has a DxR-like motif WDFL, and (C) WDR71 lacks any DxR motif. DCAF4 also has an H-box motif that may be necessary for interactions with DDB1.

Co-immunoprecipitation experiments were conducted to screen the WD40 proteins for association with the CRL4 complex. We probed for DDB1 co-precipitation because the CRL4 model shows it binds DCAFs directly (Figure 3.4B). FLAG-fusion vectors for WDR3, WDR21A.2, WDR33.3, and WDR71.1 were transfected into HEK293 cells. WDR33.3 expression was very low and potentially indicative of cytotoxicity that prevents production of high quantities of protein. The expressed proteins were FLAG purified and analyzed by immunoblotting for presence of the CRL4 subunit DDB1 that recruits DCAFs with its BPA and BPC double propeller folds [106]. Of the four WD40 genes, only WDR21A successfully co-precipitated DDB1 (Figure 3.4C). This finding

56

corroborated earlier research that identified WDR21A as the DDB1 Cullin Associated

Factor 4, DCAF4 [108].

A

B   **C**
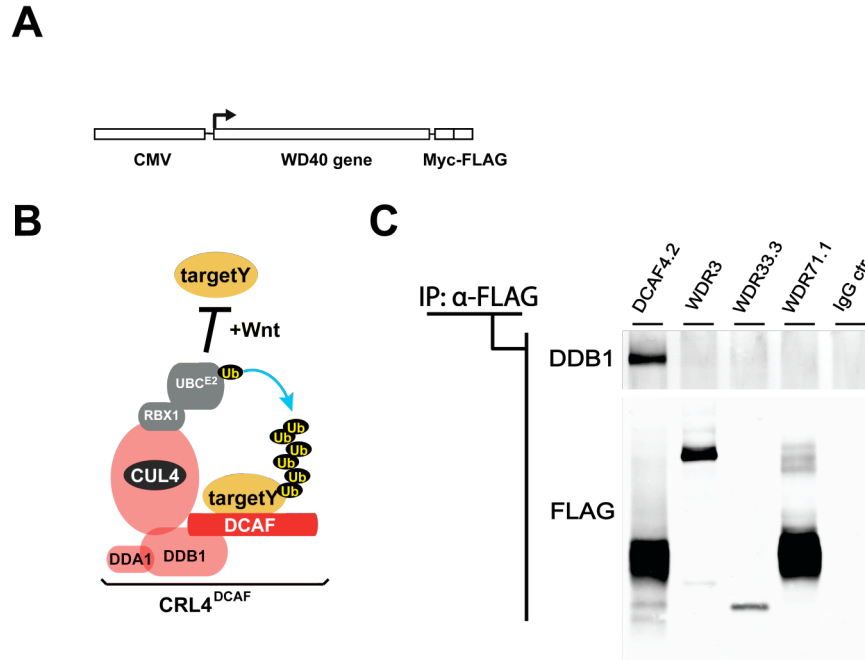
Figure 3.4 DCAF4 co-immunoprecipitates CRL4 subunit DDB1
(A) FLAG-tagged WD40 genes were expressed in HEK293 cells and then immunoprecipitated to
detect co-purified DDB1, which should directly bind DCAFs according to the CRL4 model (B).
(C) Purified samples were examined by SDS-PAGE and Western Blot to determine DDB1
co-precipitation.

DCAF4 isoform interacts with the DDB1-CUL4 E3 ligase and associated components.

while isoforms 1 and 3 fail to stably bind DDB1.

Affinity purified FLAG-DCAF4 exhibited differences in DDB1 binding depending on the

isoform (Figure 3.5). The DDB1 immunoblot normalized against the purified FLAG

signal showed a significant enrichment for DDB1 by isoform 2 compared to isoforms 1

and 3. This result was consistent in both 293 T-REx and HeLa T-Rex cell lines. Although

isoform 2 is the shortest, it is the only one to stably interact with DDB1. The WD40 and

H-box domains are conserved between isoforms 1 and 2, so the N-terminal region of

isoform 1 appears to have a negative effect on DDB1 binding. Isoform 3 shares the N-

terminal region with isoform 1 but lacks the H-box domain.
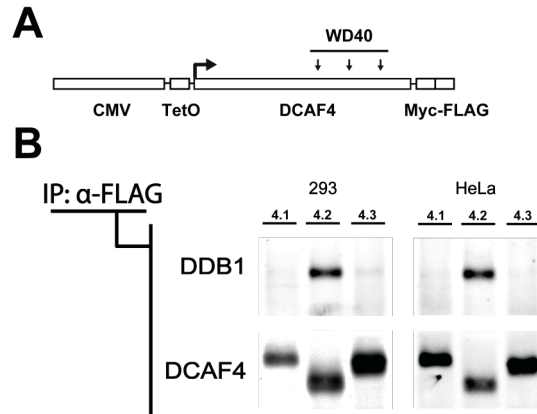
Figure 3.5 DCAF4 isoforms exhibit differential binding to DDB1 consistent in both HeLa and 293 cell lines.
(A) HeLa and 293 T-REx cell lines expressing tet inducible DCAF4 were incubated with tetracycline (200ng/mL) 16h. Cell lysates were then harvested and affinity purified with anti-FLAG beads. (B) IP elutions were analyzed by SDS-PAGE and Western Blot.

DCAF4 subcellular localization contingent on N-terminal NLS and cell type

The failure of DCAF4 isoforms 1 and 3 to co-precipitate with DDB1 could be explained if they segregated to different subcellular compartments. To examine cell localization, DCAF4 isoforms were fused with EYFP at the N terminus and transfected into HEK293-Rex, HeLa T-Rex, MCF15, and MCF7 cells. Isoforms 1-3 shared identical cytoplasmic expression in HEK293 cells despite their nuclear localization signals. In contrast, isoform 2 remained cytoplasmic in HeLa and MCF15 cells, while isoforms 1 and 3 became enriched in the nucleus (Figure 3.6). Unexpectedly, MCF7 cells had a mixed phenotype with isoforms 1 and 3 split between cytoplasmic and nuclear localization from cell to cell. Isoform 2 remained cytoplasmic in every cell line.
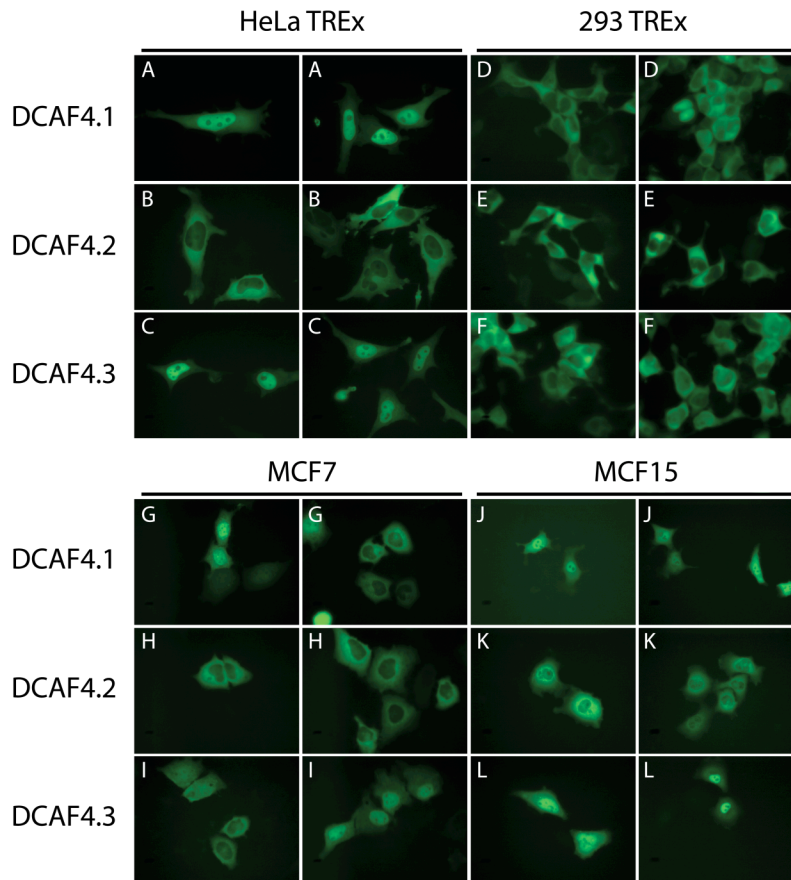
Figure 3.6 DCAF4 is differentially enriched to nucleus or cytoplasm contingent on isoform and cell line.
HeLa, 293, MCF7, and MCF15 cell lines were transiently transfected with expression vectors for N-EYFP fusion DCAF4 isoforms 1-3. Cells were observed by fluorescence microscopy to qualitatively determine subcellular localization. The vast majority of N-EYFP DCAF4 expressing cells had clear phenotypes. Each cell line and isoform combination is described by two images to account for the mixed phenotype observed in MCF7 cells.

The N-terminal domain was analyzed for structural elements with the PredictProtein online server [121]. A small N-terminal region was determined to have residues with high DNA binding potential. However, the length of this sequence is too short to realistically bind DNA on its own and is predicted to be relatively unstructured [121]. Further analysis identified a potential nuclear localization signal (NLS) within this region (RRRHGRR) [122] (Figure 3.7A).

A

N-terminal domain

B

HeLa TREx

Δ1-100

Δ2-17

Δ2-60

Δ17-60

Δ60-90
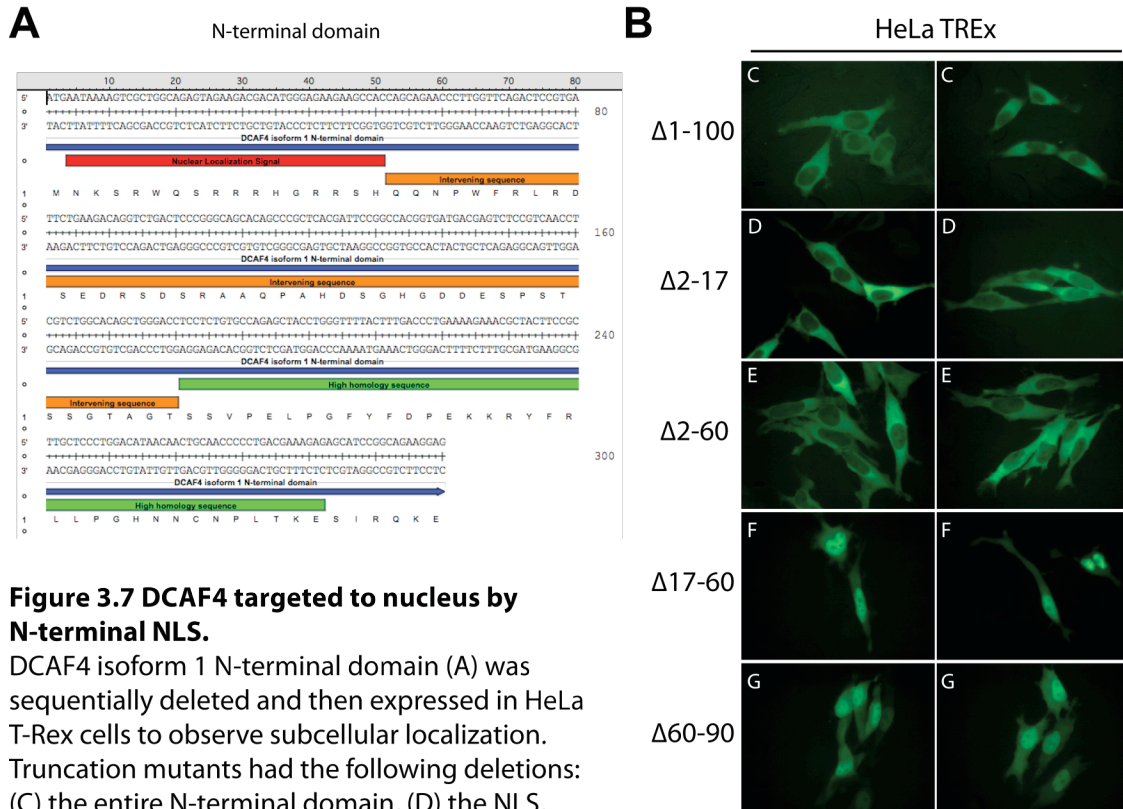
Figure 3.7 DCAF4 targeted to nucleus by N-terminal NLS.
DCAF4 isoform 1 N-terminal domain (A) was sequentially deleted and then expressed in HeLa T-Rex cells to observe subcellular localization. Truncation mutants had the following deletions: (C) the entire N-terminal domain, (D) the NLS, (E) the NLS and intervening sequence, (F) the intervening sequence alone, and (G) the high homology domain.

Multiple sequence alignment with DCAF4 homologs revealed a conserved 60-94aa region we will refer to as the high homology sequence. This region was separated from the NLS located near the start codon (2-17aa) by an intervening sequence (17-60aa). To confirm that the NLS identified on the N-terminal domain of isoforms 1 and 3 was responsible for their nuclear enrichment in HeLa and MCF15 cells, the NLS, intervening sequence, and high homology sequence were sequentially deleted to generate truncation clones. These N-EYFP fused deletion mutants were transfected into HeLa cells and examined by fluorescence microscopy. Figure 3.7B shows that nuclear DCAF4 isoform 1 expression was eliminated in mutants lacking the NLS but not in the other deletions.

Mutations to WDxR motif in WD40 domain of DCAF4 isoform 2 eliminates CRL4 binding.

Because the WD40 domains of many known DCAFs share a highly conserved WDxR motif that has been found to be important for stable association of the WD40 beta propeller structure with DDB1, it was hypothesized that mutating these residues in DCAF4 could create a dominant negative protein that stably binds to substrate but is disconnected from the polyubiquitylation machinery of the CUL4 DDB1 E3 ligase.
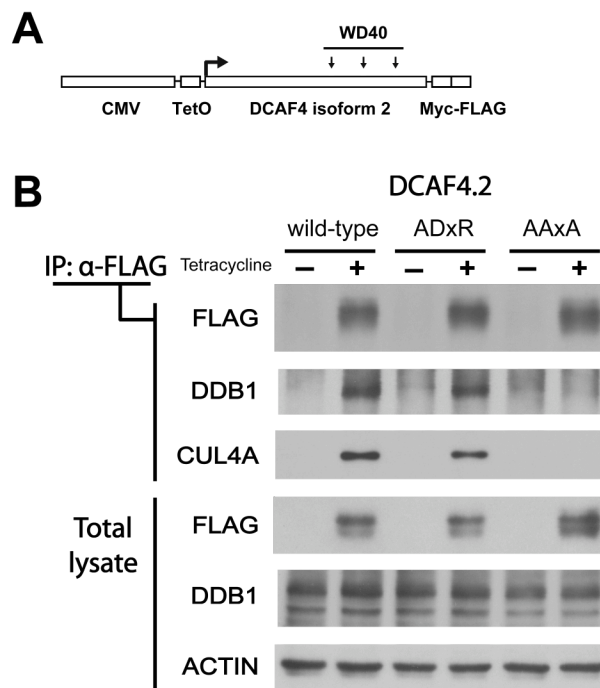
Figure 3.8 DCAF4 WDxR mutations influence DDB1 co-precipitation.
(A) HEK293 T-REx stable cell lines were incubated with tetracycline (200ng/mL) 16h to induce DCAF4 expression. Negative controls were not given tetracycline. Cell lysates were then harvested and affinity purified with anti-FLAG beads. (B) IP elutions were analyzed by SDS-PAGE and Western Blot to determine co-precipitation with CRL4 components DDB1 and CUL4A.

While the WDxR Arg residues in various DCAFs including DDB2, DCAF11, DCAF8, CSA, Cdt2, and DCAF12 were critical for DDB1 association [106, 108], a loss of DDB1

binding was not observed for DCAF4.2^{R300A} (data not shown). In Figure 3.8, DCAF4.2^{W297A} also failed to effect an observable change. Mutating the entire WDxR motif, however, was sufficient to eliminate DDB1 association.

E3 ligase substrate adaptors have been known to possess an auto-regulatory function in targeting themselves for polyubiquitylation and proteasomal turnover. We explored this possibility in DCAF4 by comparing its turnover rate for wild-type and WDxR mutant protein. 293TREx stable cell lines expressing tetracycline inducible DCAF4 were treated with cycloheximide (5ng/mL) for set time points (Figure 3.9).
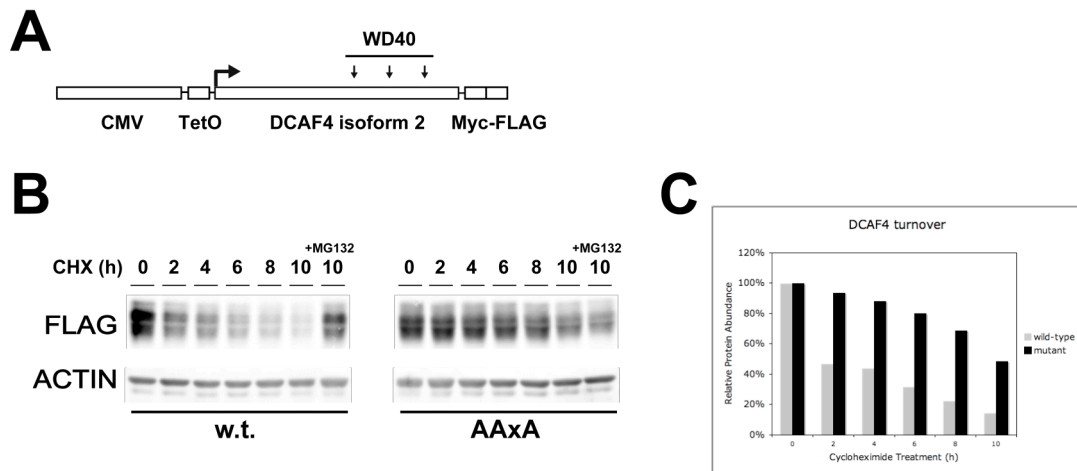
Figure 3.9 DCAF4 AAxA mutation stabilizes protein by inhibiting proteasomal turnover.
(A) HEK293 T-REx DCAF4 stable cell lines (wt/AAxA mutant) were split into identical wells and treated with tetracycline (200ng/mL) for 16h to induce maximal DCAF4 expression. (B) Cells were then washed in PBS and given fresh media containing cycloheximide (5ug/mL) to arrest protein synthesis. Cells were harvested at the indicated time points following cycloheximide incubation and then analyzed by SDS-PAGE and Western Blot. (C) FLAG-DCAF4 protein was quantified and graphed to allow comparisons of protein turnover.

We found that wild-type DCAF4 exhibited a rapid turnover rate with an estimated half-life of ~3h. The WDxR mutant, however, was far more stable with a half-life of roughly 8h. Thus, mutagenizing the WDxR motif causes a loss-of-function mutation, which gives the advantage of minimizing alterations to the overall protein structure. This allows the

mutant DCAF4 to be used as a dominant negative substrate adaptor in screening for potential substrates.

MudPit Mass Spectrometry analysis of DCAF4 isoform

MudPit mass spectrometry analysis of batch-purified wild-type and WDxR mutant FLAG-DCAF4 identified 1011 total unique proteins. While most of them were nonspecific interactions also present in the negative control sample, some interactors were known components of the CRL4 complex: CUL4A, CUL4B, DDB1, RBX1, and DDA1 (Figure 3.10).
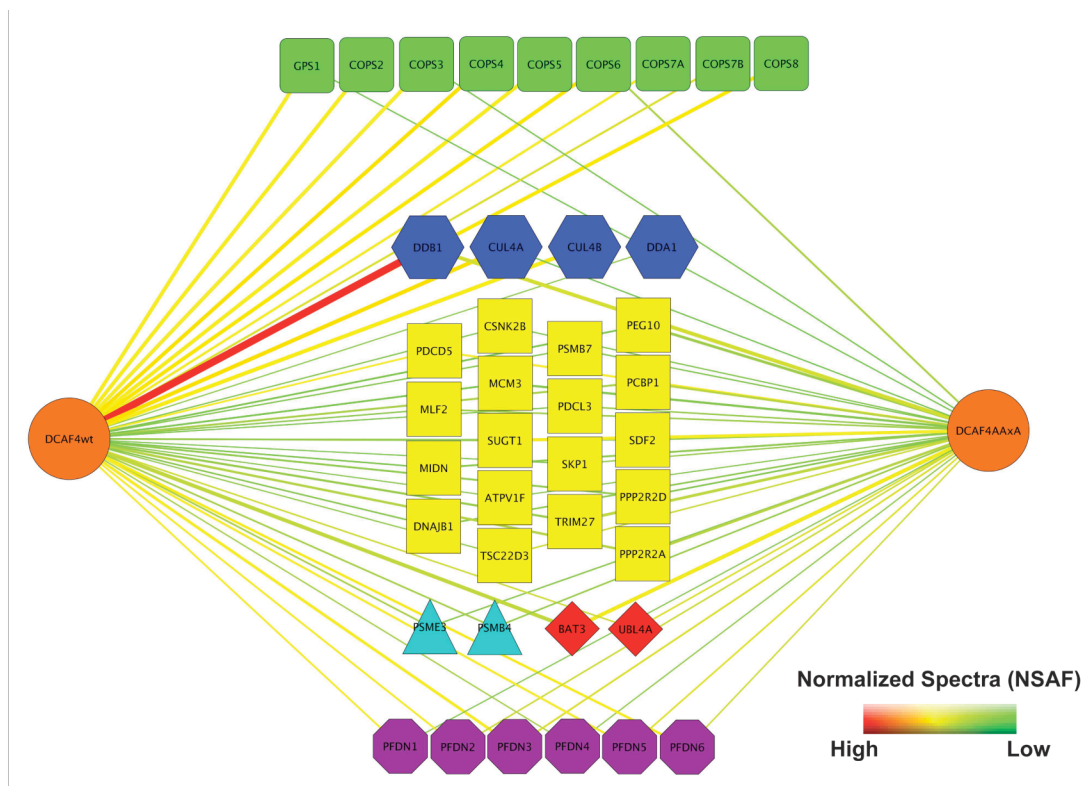
Figure 3.10 DCAF4wt and AAxA mutant MudPit interactome.
DCAF4 interaction network generated by tandem mass spectrometry analyses of affinity purified DCAF4 wild-type and AAxA mutant protein. The two DCAF4 bait proteins are marked as orange circles. Identified proteins are categorized according to known functions and associations. Components of the COP signalosome, CRL4 complex, proteasome, BAT3 complex, prefoldin complex, and miscellaneous interactors are organized by distinct colors and shapes. The statistical confidence of the protein-protein interactions are graphically delineated by the color and thickness of the connecting lines. Darker colors indicate higher NSAF scores, and the thickness of connecting lines correspond to the total spectral counts for a given interactor.

Two additional complexes were also found to be uniquely associated with DCAF4. All 9 subunits of the COP9 signalosome were enriched with the purified wild-type DCAF4 along with the 6 subunits of the prefoldin complex. The CRL4 complex and the COP9 signalosome were noticeably absent in the WDxR mutant sample set along with a reduction in the NSAF score for the prefoldin complex. The loss of CRL4 and COP9 components are entirely consistent with the current model whereby DCAFs associate with CRL4 via DDB1 while COP9 association with DCAF4 is dependent on CRL4-DCAF association [106, 123]. We also identified proteins in the dataset that failed to co-purify with known interacting partners. Many of these proteins were uncharacterized, but several were promising candidates for DCAF4 substrates due to their relationship to cell cycle and apoptosis regulation in the literature: p16INK4A, MLF2, and PDCD5. The cell cycle inhibitor p16 is frequently mutated or deleted in cancers due to its role in inhibiting CDK4 and CDK6 during G1 arrest [124, 125]. Although little is known of MLF2 outside of large-scale screens, its relative MLF1 is known to regulate stability of the tumor suppressor p53 in a concentration-dependent manner [126]. PDCD5 is involved in the caspase-3 apoptotic pathway, and its expression levels have been found to correlate with certain cancers and poor prognosis [127-129].

DCAF4.2wt overexpression and knockdown have no effect on p16INK4A, MLF2, and PDCD5 protein levels

To determine whether DCAF4 targeted p16INK4A, MLF2, and PDCD5 for proteasomal degradation, we examined the effect of DCAF4 protein expression on their steady-state protein levels (Figure 3.11). We used HEK293 T-REx stable cell lines to overexpress

DCAF4.2wt. The cells were also transfected with siRNA targeting DCAF4, DDB1, and a
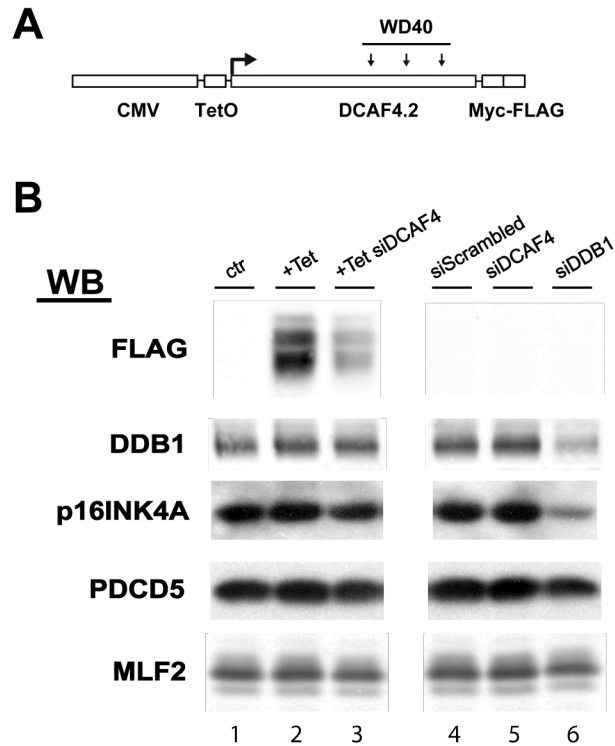
Figure 3.11 DCAF4 overexpression and knockdown has no effect on p16INK4A, PDCD5, and MLF2.
HEK293 T-REx cells expressing tet inducible DCAF4.2wt (A) were split into 6 duplicate wells. Cells were treated with a combination of tetracycline and siRNA as shown in (B) for 48h. The DDB1 knockdown was a positive control. If CRL4-DCAF4 was responsible for the turnover of a substrate, then knockdown of DDB1 should duplicate the effects of the DCAF4 knockdown. The tetracycline treated wells (2-3) were made in duplicate so one could be transfected with siRNA to DCAF4 to determine the efficiency of the knockdown.

scrambled control. Overexpression of DCAF4.2wt had no effect on p16INK4A, MLF2, or PDCD5. DCAF4 knockdown was moderately successful in reducing DCAF4 expression as observed by the noticeable downregulation of the tetracycline-induced DCAF4 protein in well 3 compared to well 2. However, DCAF4 knockdown failed to have an impact on the putative substrates. Knockdown of DDB1, on the other hand, had no effect on MLF2 and PDCD5, but did appear to reduce p16INK4A expression. According to the literature, however, this effect on p16INK4A is attributed to transcriptional regulation rather than post-translational proteasomal turnover [130].

BAT3 co-precipitation with DCAF4 requires the N-terminal region containing the UBL domain

Components of the BAT3 complex (BAT3/BAG6 and UBL4A) were enriched in the DCAF4 purifications. NSAF scores for the WDxR mutant sample were not comparatively lower than wild-type, which shows that association between DCAF4 and the BAT3 complex is not dependent on DCAF4-CRL4 binding (Table 3.1).

Gene	DCAF4.2wt Spectra	DCAF4.2wt NSAF	DCAF4.2AAxA spectra	DCAF4.2AAxA NSAF
DCAF4	586	3484	570	3267
DDB1	1325	3421	55	136
CUL4A	156	605	3	11
COPS4	80	580	0	0
COPS6	55	495	11	95
COPS8	34	478	0	0
PFDN6	17	387	6	131
CUL4B	117	384	0	0
COPS5	43	378	0	0
COPS2	54	358	0	0
GPS1/COPS1	56	335	3	17
PFDN3	22	328	10	144
PFDN5	14	267	8	147
COPS3	38	264	4	26
PFDN1	10	241	2	46
PDCD5	10	235	13	295
COPS7A	17	181	0	0
COPS7B	13	144	0	0
UBL4A	7	131	8	144
BAT3	46	119	66	165
PPPR2RA	16	105	17	107
CDKN2A	5	94	7	127
PSME3	8	92	5	55
PCBP1	11	90	14	111
PSMB4	8	89	7	75
PFDN4	4	87	3	63
TRIM27	13	74	21	116
SUGT1	9	72	26	202
TSC22D3	3	65	6	127
PPP2R2D	10	64	7	43
MLF2	5	59	7	80
DDA1	2	57	0	0
SDF2	4	55	4	53
DNAJB1	6	51	7	58
UBA2	11	50	6	26
PEG10	9	37	20	80
MIDN	6	37	10	60
PDCL3	3	36	6	71
SKP1	2	36	4	69
CDC2	3	29	6	57
HSP90AA4P	0	0	14	95
YWHAH	0	0	8	92
COX6B1	0	0	2	65
DHFR	0	0	4	60
TXNDC9	0	0	4	50
FAM127A	0	0	2	50

Table 3.1 MudPit mass spectrometry analysis of purified DCAF4.
DCAF4wt and AAxA mutant proteins were purified by anti-HA immunoprecipitation and analyzed by tandem mass spectromy. Nonspecific interactions found in the negative control were removed along with NSAF scores below 50. List is organized by decreasing NSAF score in the DCAF4.2wt sample.

To determine the specificity of the DCAF4-BAT3 interaction, we obtained expression vectors for truncated HA-BAT3 ΔN380 and ΔC482 from Desmots et al who studied BAT3 functions in apoptosis [131]. The ΔN380 truncation was missing the ubiquitin-like

domain (UBL), while the ΔC482 lost the BAG domain and NLS. We co-expressed HA-
BAT3 ΔN380 or ΔC482 with FLAG-DCAF4 isoforms 1 and 2 wild-type (Figure 3.12A).
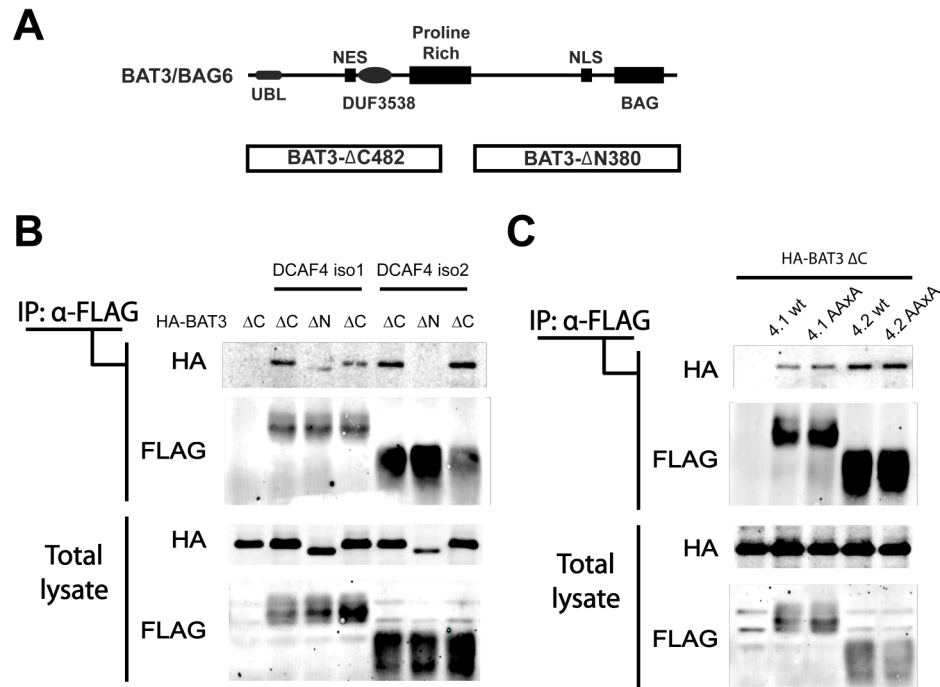
Figure 3.12 N-terminal domain of BAT3 is required for DCAF4 association.
HEK293 T-REx TetO FLAG-DCAF4 stable cell lines (isoforms 1 & 2) were transfected with (A)
HA-BAT3 ΔC or ΔN expression vectors. (B) 24h post-transfection, cells were treated with
tetracycline to induce FLAG-DCAF4 expression. 24 following tetracycline incubation, cells were
lysed, and DCAF4 was purified with anti-FLAG beads. IP elutions were analyzed by SDS-PAGE and
Western Blot for HA-BAT3 co-precipitation. (C) After HA-BAT3 ΔC was found to bind DCAF4,
DCAF4 AAxA mutants were tested for binding with BAT3 ΔC.

Affinity purification of FLAG-DCAF4 revealed that while ΔC482 BAT3 successfully co-
precipitated with DCAF4, the N-terminal deletion in BAT3 eliminated this interaction.
Knowing that HA-BAT3 ΔC still interacted with DCAF4, we co-expressed it with
DCAF4 wild-type and WDxR mutant (isoforms 1, 2) and repeated the
immunoprecipitation (Figure 3.12B). HA-BAT3 ΔC successfully co-precipitated with
purified FLAG-DCAF4 with no observable differences between the isoforms or WDxR
mutations.

BAT3 and DDB1 are enriched in partially overlapping distributions of molecular weight fractions with DCAF4

We sought to determine whether BAT3 was a major component of the CRL4^{DCAF4} complex by observing their degree of enrichment into the same molecular weight fractions. Superose 6 fractionation was performed on both total protein lysate and FLAG affinity purified DCAF4 isoform 2.
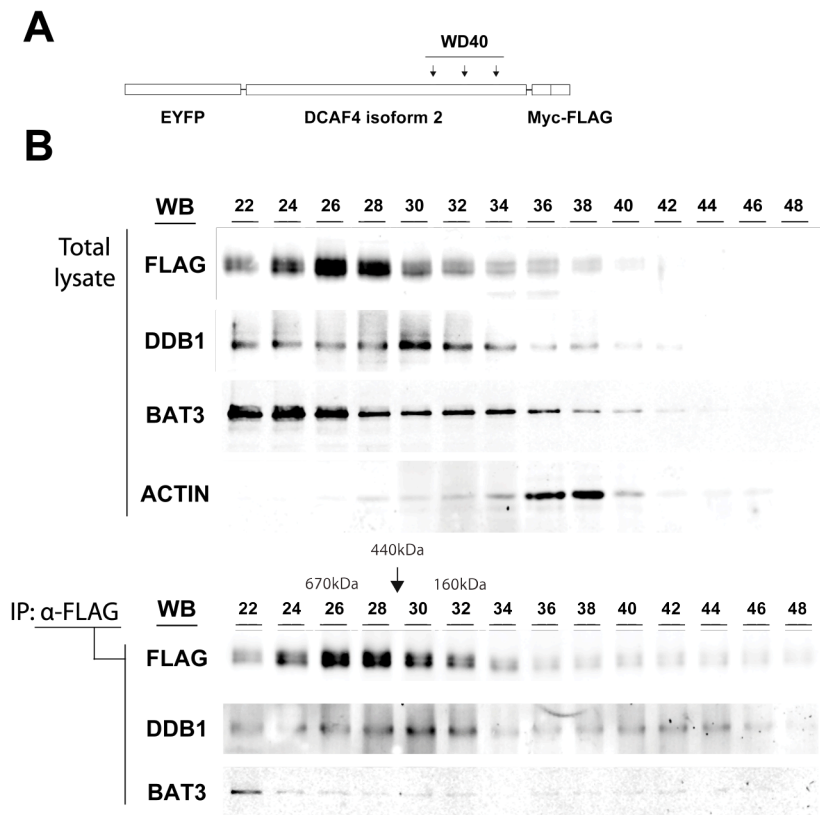
Figure 3.13 DCAF4.2 co-localization with DDB1 and BAT3.
(A) DCAF4.2 was expressed in HEK293 T-REx cells and the lysate fractionated by gel filtration (superose-6 fractionation). The fractions were examined for FLAG-DCAF, DDB1, BAT3, and ACTIN protein expression by Western Blot. (B) DCAF4.2 lysate was immuno-purified with anti-FLAG beads, and the elution fractions were separated and analyzed as in (A).

The total lysate fractions revealed that DCAF4, DDB1, and BAT3 were enriched into partially overlapping fraction distributions with DCAF4 and DDB1 experiencing significant overlap while BAT3 was more concentrated in higher molecular weight

68

fractions (Figure 3.13A). By comparison, the purified fractions had a similar profile in which the amount of co-precipitated DDB1 and BAT3 were reflective of their total lysate expression (Figure 3.13B). BAT3 was more enriched in the higher molecular weight fraction than DDB1, but there was still some degree of co-precipitation with DCAF4 in the same fractions.

Prefoldin Complex

Components of the prefoldin complex were also detected in both wild-type and mutant DCAF4 samples. There appeared to be a drop in relative NSAF scores for prefoldin components in the mutant sample dataset (Table 3.1). To both confirm this interaction and to show that mutant DCAF4 had lower affinity for prefoldin subunits, we examined co-immunoprecipitation of prefoldin 5 with wild-type and mutant DCAF4 isoforms 1 and 2. Western Blot revealed that wild-type successfully pulled down prefoldin 5 and that the WDxR mutation significantly reduced this interaction (Figure 3.14B). Since the prefoldin complex is a chaperone, this interaction may be the result of prefoldin mediating DCAF4 folding. To determine whether prefoldin binds DCAF4 only during protein folding, we treated cells with cycloheximide for 4h to arrest protein synthesis. Proteasome inhibitor MG132 was also added to prevent DCAF4 from being degraded. The extracts were then immunoprecipitated for DCAF4 and analyzed by Western Blot. Prefoldin 5 enrichment was unchanged by cycloheximide treatment (Figure 3.14C).
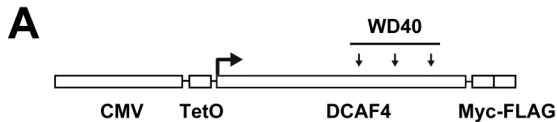
Figure 3.14 Prefoldin 5 binding with DCAF4 depends on WDxR motif.
(A) HEK293 T-REx stable cell lines expressing tet-inducible DCAF4 variants were used to perform co-immunoprecipitation experiments to determine prefoldin 5 association with DCAF4. (B) Prefoldin 5 association was assayed in DCAF4 isoforms 1/2 wild-type/AAxA mutant. (C) Prefoldin 5 binding was also assayed following 4h cycloheximide treatment that arrests protein synthesis to determine whether DCAF4-prefoldin binding occurred during protein synthesis or later.
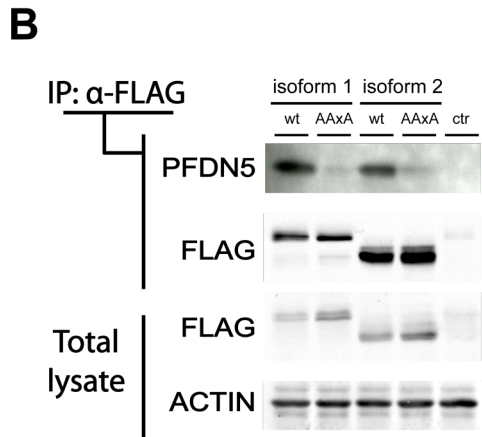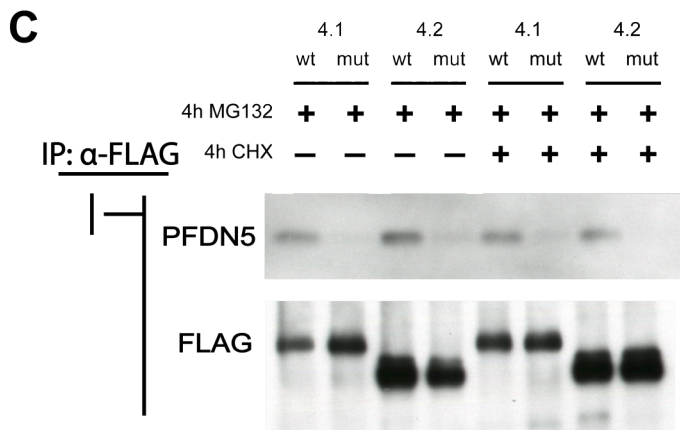
DCAF4 doublet is not caused by phosphorylation

Multiple Western Blots of DCAF4 have found that it migrates as a doublet centering on its predicted molecular weight of 45-55kDa (varies between isoforms). In our previous work on p27, we found that p27 frequently migrates as a doublet and that the upper band is attributed to a phosphorylation in the literature. We wanted to determine whether the DCAF4 doublet could be explained in the same manner since phosphorylation status could be functionally relevant. Therefore, we treated DCAF4 protein extract with CIP and examined the doublet by Western Blot (Figure 3.15). While phospho-473S Akt was

completely absent compared to the control, confirming successful de-phosphorylation by CIP, there was no effect on the DCAF4 doublet.
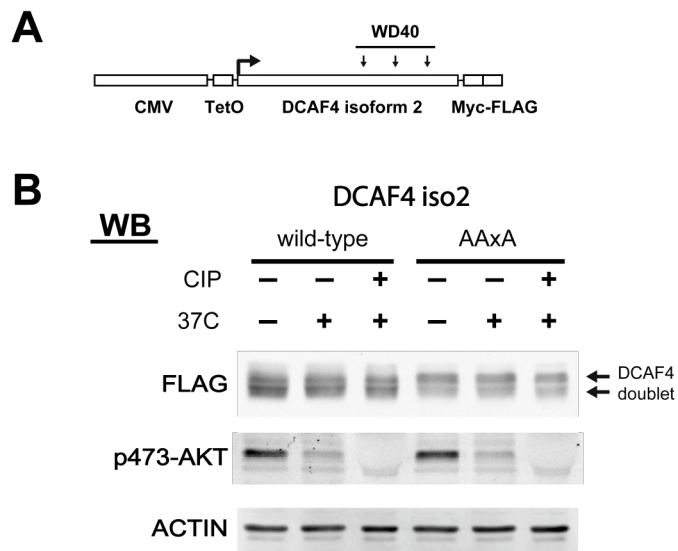
Figure 3.15 DCAF4 SDS-PAGE migration doublet is not caused by phosphorylation.
(A) HEK293 T-REx stable cells were treated with tetracycline (200ng/mL) to induce DCAF4 expression for 16h. (B) Cell lysates were harvested for isoform 2 wild-type and AAxA mutant cells in lysis buffer with or without phosphatase inhibitors. Samples extracted without phosphatase inhibitors were incubated for 30min at 37C or with CIP at 37C to catalyze protein dephosphorylation. Extracts were then analyzed by SDS-PAGE and Western Blot. Phospho-473 Serine AKT immunoblot was performed to control for efficiency of CIP dephosphorylation.

3.4 Discussion

Wnt signaling regulates diverse processes including cell proliferation, cell fate, and stem cell maintenance [17]. Its regulatory function is achieved through the modulation/induction of numerous downstream Wnt target genes, many of which have key regulatory roles in critical cellular processes themselves [17]. The relationship between Wnt signaling and the ubiquitin proteasome system has mostly centered around the various ways in which ubiquitylation acts to regulate components of the Wnt signaling pathway, most notably the SCF targeting of beta catenin for polyubiquitylation and proteasomal degradation [132]. Relatively little work has focused on the influences of Wnt signaling on ubiquitylation. Our work has examined Wnt modulation of WD40

gene expression including a known DCAF that is predicted to polyubiquitylate substrates as part of the CRL4 complex. We have confirmed DCAF4 as a DDB1 CUL4 E3 ligase associated protein consistent with the literature [106, 108]. We have revealed a number of novel DCAF4 associated proteins by MudPit mass spectrometry analysis of wild-type and dominant negative DCAF4 with the most interesting being components of the BAT3 complex. Our findings have yielded insight into potential functional relationships between CRL4^{DCAF4} and the BAT3 and prefoldin complexes.

Wnt modulation of WD40/DCAF expression

Wnt modulation of ubiquitylation can be inferred from its involvement in various cellular processes. For example, the mitogenic effect of beta catenin stabilization can lead to cell cycle progression and division, which have been well established to involve the targeted ubiquitylation of cyclin/CDK inhibitors such as p16, p21, p27, and p53. Specifically, earlier research has revealed a Wnt10b-induced E3 ligase CRL4 that targets p27 for degradation in an alternate targeting mechanism to the previously characterized SCF^{SKP2} E3 ligase [70]. The Wnt induction of CRL4 core components to modulate p27 turnover led to the investigation of Wnt modulated WD40 genes to discover potential DCAFs that could have downstream functions of active Wnt signaling. Real time PCR analysis of DLD1 cells over-expressing the dominant negative TCF1E corroborated microarray data (Waterman comm.) for WDR3, WDR21A, and WDR71 but not WDR33 (Figure 3.2).

Wnt activation using lithium chloride in MCF15 mammary cells, on the other hand, showed a modest induction of WDR3, WDR21A, and WDR33 with no change to WDR71. The divergent results may be explained by the use of different mechanisms for modulating the Wnt pathway and the use of cell lines with fundamentally distinct origins.

While TCF1E can compete with endogenous TCF1 for Wnt target genes, it will not account for the remaining Wnt transcription factors LEF1, TCF2, and TCF4. Lithium chloride, meanwhile, is an inhibitor of GSK3 beta, which acts to phosphorylate beta catenin and target it for polyubiquitylation and degradation. Consequently, lithium chloride inhibition will lead to beta catenin activation, nuclear translocation, and unrestricted association with downstream Wnt transcription factors [133, 134]. These considerations may explain the irregularities in WDR33 and WDR71 expression.

WDR21A validated as DCAF4

While Wnt modulation of WD40 genes in general is interesting, we focused our investigations on their potential functions as DDB1 CUL4 Associated Factors (DCAFs). The canonical amino acid sequences for these genes revealed multiple WD40 domains (Figure 3.3). WDR3 contained a WDxR motif within its N-terminal WD40 domain that was highly conserved amongst known DCAFs, while this motif was not present in both WDR33 and WDR71. WDR21A also shared this WDxR motif and had been previously identified as DCAF4 [106, 108, 135]. Immunoprecipitation of FLAG-tagged WD40 proteins confirmed WDR21A as the only DDB1 associated protein (Figure 3.4). Thus, the WDxR motif in WDR3, while highly conserved and found to be important for mediating binding of the WD40 beta propeller surface to DDB1, did not correlate with DCAF status in this case. One caveat of our finding is that not all DCAFs will necessarily be associated with DDB1 in every cellular context. It is entirely possible that certain DCAF-DDB1 interactions will be present in only a subset of cell types under distinct cellular conditions.

DCAF4 isoforms & functional differences

DCAF4 has multiple splice isoforms that share the conserved C-terminal exons containing three WD40 domains with most of the splice variation centering on the N-terminal domain (Figure 3.3). We focused on the three isoforms (1-3) that exhibit significant sequence divergence. DCAF4 isoform 1 is 495aa with a 100aa N-terminal domain that is spliced out in isoform 2. Isoform 3 retains the N-terminal domain but has a downstream exon spliced out. Taken together, they offer endogenous variants on DCAF4 sequence that could have implications for function. Co-immunoprecipitation experiments revealed that only isoform 2 is capable of co-precipitating DDB1 (Figure 3.5). Because isoforms 1 and 3 share a common N-terminal domain that is missing in isoform 2, the data suggests that this particular domain has an inhibitory function on DCAF association with the core CRL4.

Sequence analysis shows that isoforms 1 and 3 feature a bipartite nuclear localization signal (NLS) within their N terminal domain that suggested DDB1 association could be dependent upon nuclear import (Figure 3.7A). N-terminally fused EYFP-DCAF4 expressed in 293 T-REx cells revealed that every isoform was observed predominantly in the cytoplasm. Even more interesting was the discovery that DCAF4 expression displayed distinct cell localization profiles depending on the cell line it was expressed in (Figure 3.6). While DCAF4 remained cytoplasmic in the fibroblastic HEK293 cell line, isoforms 1 and 3 were enriched in the epithelial HeLa TREx and MCF15 cell lines. Even more unexpected was the mixed phenotype in the mammary MCF7 epithelial cell line with an even division between nuclear and cytoplasmic DCAF4 (isoforms 1 and 3). The only constant was isoform 2, which remained cytoplasmic. The NLS was verified when N-terminal deletions to DCAF4 isoform 1 confirmed the loss of

nuclear localization in the truncated DCAF4 protein lacking the 2-17 amino acids located at the N-terminus (Figure 3.7B).

However, the differences in DDB1 co-precipitation bear no relation to differences in cellular localization since those experiments were conducted in 293Rex cells in which every isoform were found in the cytoplasm. Furthermore, co-IP experiments using HeLa cells gave the same results as with the HEK293 cell line, and isoform 2 continued to be the only one to successfully pull down DDB1. This finding opens up the possibility that isoforms 1 and 3 operate in a natural dominant negative role in which they bind substrate without catalyzing ubiquitylation. In this context, alternative splicing of DCAF4 could be a mechanism for fine-tuning the ubiquitin-dependent proteolysis of CRL4 targets.

Dominant negative DCAF4Because only isoform 2 was capable of co-precipitating CRL4 components, we utilized this particular clone for tandem mass spectrometry analysis of DCAF4 associated proteins in an attempt to identify possible ubiquitylation substrates. We sought to mutagenize isoform 2 and generate a dominant negative that we could analyze alongside the wild-type in order to identify substrates that would theoretically become protected from degradation and form a stable interaction with DCAF4. The strategy for generating a dominant negative DCAF4 was to eliminate association with the CRL4 core complex while retaining substrate binding. While this can be achieved by simply deleting one or more WD40 beta propeller domains that are required for DDB1 binding, large alterations to protein sequence can result in structural defects that prevent functional interactions with the substrate itself. For example, removal of a binding surface can expose previously hidden hydrophobic surfaces that result in decreased solubility and increased misfolding or protein aggregation. This defect can be

rectified with additional point mutations that convert exposed hydrophobic residues into hydrophilic ones to increase solubility, but such a strategy can be time consuming [136].

Fortunately, we learned from the established literature that the conserved WDxR motif in DCAFs was necessary for stable binding between their WD40 beta propeller fold and the BPA-BPC beta propeller surfaces on DDB1, although this was not the case for every DCAF [106]. Mutating this motif in DCAF4 successfully eliminated binding with CRL4 core subunits DDB1 and CUL4A (Figure 3.8). We found further support that mutating the WDxR motif would generate a dominant negative by observing that proteasome-dependent turnover of the mutant was significantly slower compared to the wild-type (Figure 3.9). These findings allowed us to move onto the mass spectrometry screen for unknown binding partners.

DCAF4 CRL4 interacting partners

CRL4 core subunits DDB1, CUL4A, CUL4B, and DDA1 were identified in the DCAF4 MudPit dataset (Figure 3.10). The normalized spectral abundance factor (NSAF) scores were highest for DDB1, which is to be expected given that DCAF4 is predicted to directly bind DDB1 (Table 3.1). Of some interest was the presence of both CUL4A and CUL4B since they would not be found in the same CRL4 but rather as distinct complexes. However, since DDB1 acts as the physical bridge between DCAFs and CUL4, it may simply be expected that DCAF4 would be associated with both cullins. Regardless, it may be difficult to discern biological distinctions between the two CRL4^{DCAF4} complexes since there is considerable functional overlap between CUL4A and CUL4B. In line with our observations, the WDxR mutant DCAF4 had a dramatic reduction in NSAF for DDB1, CUL4A, CUL4B, and DDA1.

The presence of the 9 subunits of the COP signalosome confirmed Wade Harper's COMPASS dataset showing that DCAF4 was present in the COPS5 and COPS6 subunits [137]. Our data demonstrated that this interaction required DDB1 binding since the COP signalosome was noticeably absent from the WDxR mutant dataset. Furthermore, DCAF4 is enriched in gel filtration fractions between the molecular weights of 440 and 670kDa, which parallel the distribution of COP signalosome subunits [138]. It is important to note that not all DCAFs or F-box proteins associated with Cullin Ring Ligases have been found to interact with COP signalosome at a sufficient stability for detection. For example, only certain F-box and WD40 proteins have been found to have significant associations with the COPS5 and COPS6 subunits in mass spectrometry screens: DDB2, FBXO17, VPRBP, WDR23, FBXO1, SKP2, FBXW9, FBXO11, FBXO44, DTL and FBXO22 [137]. This is in contrast to screens using CUL4 and DDB1 as bait, which identified dozens more WD40/WDR proteins as DCAFs [106, 108, 135, 139]. Thus, the strong association between CRL4^{DCAF4} and the COP signalosome hints at underlying molecular dynamics that remain to be more fully characterized.

In addition, components of the 26S proteasome have also been detected. This may not be surprising given the close association of CRLs with the proteasome for mediating protein turnover. CRL4^{DCAF4} could be associated with the proteasome via tertiary interactions.

DCAF4 novel interactions

While our screen initially identified several potential substrates in the form of PDCD5, MLF2, and p16, follow-up experiments failed to yield evidence for DCAF4-mediated turnover. This raises a key concern of such screens in that it is difficult to sift out true hits from false positives. None of these putative substrates had compellingly high NSAF

scores, but were high enough with potentially interesting biology to warrant attention. Furthermore, they were not identified together with known interacting partners that would lend greater credence to the idea of a specific interaction rather than nonspecific background contamination. On the other hand, two novel complexes were discovered in our screen: the prefoldin complex and the BAT3 complex.

Prefoldin complex

The prefoldin complex was originally identified as a hexameric chaperone complex that functioned together with cytosolic chaperonin to mediate de novo protein folding [140]. While its chaperone functions were diverse in archaea, the prefoldin complex is identified as having the much more specific task of folding beta actin in eukaryotic cells by binding & transporting unfolded actin to cytosolic chaperonin [140, 141]. While most of the literature focuses on the complex's chaperone function, one of its subunits prefoldin 3 or VBP1 has been shown to bind to the von Hippel Lindau substrate adaptor of the $CUL2^{VHL}$ ubiquitin ligase [142]. VBP1 appears to serve as a middleman in targeting the viral enzyme HIV-1 integrase to the $CUL2^{VHL}$ complex for polyubiquitylation and degradation [142].

The Drosophila prefoldin subunit Mgr has also been implicated together with Vhl in regulating tubulin stability, and the findings suggest that Vhl promotes Mgr-dependent turnover of misfolded tubulin [143]. Since Vhl depletion leads to loss of meiotic spindle integrity characterized by monopolar spindle formation and centrosomal loss, the prefoldin complex is crucial to spermatogenesis [143]. This finding is particularly relevant considering that CUL4A knockout mice are severely defective in spermatogenesis with gross abnormal morphology and near total loss of postmeiotic cells

in the testes [144]. These findings reveal an unexpected side of the prefoldin complex that has not been well characterized and raises intriguing possibilities for the DCAF4-prefoldin interaction in cytoskeletal dynamics.

BAT3 complex

Our screen also yielded two subunits of the BAT3 complex: BAT3/BAG6 and UBL4A. The BAT3 complex plays a key quality control role in transmembrane protein folding as part of ERAD [145]. BAT3 was first identified as a chaperone that acts as an intermediary in shuttling nascent transmembrane proteins between ribosomes and the endoplasmic reticulum [146, 147]. The BAT3 complex bound misfolded proteins with exposed hydrophobic residues [146]. If these tail anchored proteins failed to handoff from BAT3 to the transmembrane domain recognition complex (TRC) for insertion and assembly in the ER, they are polyubiquitylated and sent to the proteasome for proteolysis [148, 149]. BAT3 has been hypothesized to associate with E2 and E3 ligases that polyubiquitylate BAT3-bound substrates, but the identities of these E3 ligases are not well characterized. Thus far, the ER-associated E3 ligase gp78 has been shown to bind BAT3 via its ubiquitin-like domain (UBL) [145].

However, the dispersed cytoplasmic expression of DCAF4 in HEK293 cells does not match the immunofluorescence profile of the Endoplasmic Reticulum, and there is no evidence that CRL4^{DCAF4} plays a functional role as an E3 ligase in ubiquitylation of BAT3-associated misfolded ER proteins. This function already has a viable candidate in the form of gp78, and although functional redundancies via additional E3 ligases are certainly possible, known ERAD E3 ligases found predominantly in the ER are more plausible. Furthermore, the available literature indicating BAT3's involvement in diverse

molecular processes coupled with its ubiquitous presence across multiple cellular compartments (nuclear, cytoplasmic, ER) could make the CRL4-BAT3 relationship challenging to isolate. Even so, there are several reasonable avenues for further exploration.

BAT3 and the UPS

BAT3 has been connected with the ubiquitin-proteasome pathway repeatedly in the literature. It has been found to be targeted for ubiquitylation by the SCF complex during Legionella pneumophila infection with the pathogen supplying the F-box substrate adaptor LegU1 that hijacks the SCF complex [150].What function this serves is unclear. However, BAT3 depletion has been shown to confer resistance to apoptosis and ER stress [131, 151]. This function may be due in part to its proteolytic activation by caspase-3, which cleavages BAT3 into a truncated fragment CTF-131 that catalyzes apoptotic pathways leading to phosphatidylserine exposure and chromatin condensation [152]. Interestingly, Legionella pneumophila infected macrophages show activation of caspase-3 and yet are resistant to apoptosis [153]. Given this evidence, it is reasonable to hypothesize that Legionella F-box protein LegU1 targets BAT3 to prevent infected cells from becoming apoptotic as part of an immune response against the pathogen.

The observation that bacterial F-box proteins could target BAT3 for ubiquitylation suggests that endogenous host E3 ligases may share this function. This raises the question of whether the SCF complex possesses endogenous ability to target BAT3. For instance, the F-box protein SGT1 has been identified as a BAT3 interacting protein in a yeast-2-hybrid screen [154]. SGT1 is an F-box protein and substrate adaptor for the SCF E3 ligase and is required for proper kinetochore assembly [155]. Its

interaction with the BAT3 UBL domain suggests a functional relationship between BAT3 and SCF. Both appear to be involved with the immune response. As a gene located in the MHC class III region of the genome, BAT3's role in protein folding quality control could be significant with regards to peptide processing for antigen presentation, which offers insight into why Legionella pneumophila targets BAT3 for ubiquitylation. Similarly, SGT1 interacts with Nod-like receptors (NLRs) to take part in the innate immune inflammasome response [156].

Interestingly, SGT1/SUGT1 was identified in our DCAF4 mass spectrometry analyses. Its presence was not only undiminished in the WDxR mutant sample but was significantly higher with 26 spectra and 15 unique peptides compared to the 9 spectra and 6 unique peptides in the wild-type sample. The noticeable stabilization of SGT1 co-purification with dominant negative DCAF4 suggests their respective E3 ligase complexes may be involved in regulating one another. As a comparison, the F-box protein SKP2 is polyubiquitylated by the anaphase promoting complex APC^{CDH1} during cell cycle progression and TGF-beta induced arrest [157, 158]. However, whether DCAF4 or SUGT1 target each other or if they both independently target BAT3 or BAT3 substrates for ubiquitylation is a question that remains to be addressed.

Potential DCAF4-BAT3 functional interactions

The diverse array of BAT3 associated functions could explain why we do not see a stronger correlation in the enrichment of BAT3 and DDB1 in DCAF4 pulldown fractions. If BAT3 is responsible for binding to misfolded substrates and then transferring them to multiple, distinct E3 ligases for ubiquitylation, then its presence could be subdivided amongst multiple molecular weight fractions based on secondary and tertiary

interactions. This explanation reconciles the enrichment of DCAF4 and BAT3 into only partially overlapping distributions of superose 6 molecular weight fractions. Whatever purpose they share together may only account for a minority percentage of their overall functions respectively. Another consideration is that their cooperation may be context specific and depends upon the cell line and activation of particular molecular pathways.

In addition, BAT3 has several alternative splice isoforms with both cell-type specific expression and subcellular distribution. Full length endogenous BAT3 was cytoplasmic in Raji cells but displayed a mixed cytoplasmic and nuclear phenotype in other cell lines, which matched our data on BAT3 expression in HeLa and MCF15 cells. Researchers also found that deletion of exon 11B led to cytoplasmic localization in the Crm1-dependent nuclear export pathway, while other isoforms were retained in the nucleus [159]. This is intriguingly similar to what we know about DCAF4, which also displays subcellular localization contingent upon the cell line and splice isoform (Figure 3.6). Unfortunately, due to the limited coverage of unique BAT3 peptides in our mass spectrometry dataset, we were unable to ascertain which BAT3 isoform co-purified with DCAF4.

While it appears unlikely that DCAF4 would be involved in the ERAD pathway with BAT3 given its context-dependent nuclear enrichment and overall lack of ER localization as ascertained by fluorescence microscopy, it is important to note that BAT3 requires the UBL containing N-terminal domain for binding to both the ER ubiquitin ligase gp78 and DCAF4. This N-terminal domain on BAT3 is also the bait that interacted with SGT1 in the yeast-2-hybrid screen that first linked those together [154]. That the BAT3-E3 ligase association is domain specific implies BAT3 is capable of recruiting

additional ubiquitin ligases through its UBL domain as a universal adaptor for proteins with UBL-binding motifs.

Also intriguing is the involvement of BAT3 in spermatogenesis since both the prefoldin complex and CUL4A play crucial roles in the same process. Bat3 inactivation in mice leads to apoptosis in male germ cells and male sterility [160]. Unlike with the prefoldin complex, BAT3 has not been implicated in tubulin stability. Instead, researchers found that BAT3 deficiency led to polyubiquitylation and proteasomal degradation of HSP70-2. In this way, BAT3 can have a protective function in addition to its involvement in shuttling substrates to the ubiquitin proteasome system.

Concluding remarks

We have confirmed DCAF4 to be a component of the CRL4 complex that is capable of auto-regulation in a proteasome-dependent manner. We found that DCAF4 is associated with a number of complexes that provide clues to its potential function. While the COP signalosome was predicted to be in our mass spectrometry dataset, we also identified the novel prefoldin and BAT3 complexes. Both appear to have distinct chaperone functions in mediating protein folding. The prefoldin complex is specialized in folding the cytoskeletal protein beta actin, although it has been implicated in regulating the turnover of substrates by conjugating them with E3 ligases. The BAT3 complex is involved in diverse pathways that include apoptosis, spermatogenesis, and ERAD.

The association of DCAF4 with two distinct chaperone complexes with unique functions suggests a role in regulating protein folding in quality control pathways. Further investigation would entail more directed research using established experimental systems best suited for studying protein folding. Furthermore, despite the differences

between the prefoldin and BAT3 complexes, they do share a common phenotype with Cullin4 in that all three are essential for spermatogenesis. If DCAF4 is to be studied any further, it may be worthwhile to generate a knockout mouse line to examine potential defects in testes and germ cell development. Hopefully, our research has laid the groundwork for such future explorations.

APPENDIX A

Table A.1

Primers	5' --> 3' sequence
p27 Y74F F	ACAAACCCCTAGAGGGCAAGTTCGAGTGGCAAG
p27 Y74F R	CTTGCCACTCGAACTTGCCCTCTAGGGGTTTGT
p27 Y88F F	CTTGCCCGAGTTCTTCTACAGACCCCCGC
p27 Y88F R	GCGGGGGTCTGTAGAAGAACTCGGGCAAG
p27 Y88F Y89F F	TTGCCCGAGTTCTTCTTCAGACCCCCGCGG
p27 Y88F Y89F R	CCGCGGGGGTCTGAAGAAGAACTCGGGCAA
DCAF4.1 del2-17F F	ATCGCCATG*CAGCAGAAC*CCTTGGTTCAGACTCCGTGATTCTGAAGAC
DCAF4.1 del2-17R R	*GTTCTGCTG*CATGGCGATCGCGGCGGCAGATCTCCTC
DCAF4.1 del61-94F	GCTGGGACC*AGCATCCGG*CAGAAGGAGATGGAGAGCAAGAGACTGCGG
DCAF4.1 del61-94R	*CCGGATGCT*GGTCCCAGCTGTGCCAGACGAGGTTGACGGAGACTC
DCAF4.1 del17-60F	AGAAGCCAC*TCCTCTGTG*CCAGAGCTACCTGGGTTTTACTTTGACC
DCAF4.1 del17-60R	*CACAGAGGA*GTGGCTTCTTCTCCCATGTCGTCTTCTACTCTGC
DCAF4.1 del2-60F	ATCGCCATG*TCCTCTGTG*CCAGAGCTACCTGGGTTTTACTTTGACCC
DCAF4.1 del2-60R	*CACAGAGGA*CATGGCGATCGCGGCGGCAGATCTCCTC
DCAF4.1 del351-533F	TCCAGGAAGAAGACAGACGGAAAAAGGCAGATACCAAC
DCAF4.1 del351-533R	GTTGGTATCTGCCTTTTTCCGTCTGTCTTCTTCCTGGA
EYFP SfaI F	TAGTTAGCGATCGCATGGTGAGCAAGGGCGAGGAGC
EYFP SfaI R	TAGTATGCGATCGCCTTGTACAGCTCGTCCATGCCGAG
TetO F	GTCCCTATCAGTGATAGAGATCTCCCTATCAGTGATAGAGACTTAAGCAGCT
TetO R	GCTTAAGTCTCTATCACTGATAGGGAGATCTCTATCACTGATAGGGACAGCT

Real Time PCR primers	5' --> 3' sequence
WNT10B	GTGGGGCGCCAGGTGGTAAC
WNT10B	CCCCCACTGCCCGGAACTCT
AXIN2	GGAGATCGAGGCGGAGGCCA
AXIN2	GCCTCTGCTGCCGCCAAACT
B2M	TGCTGTCTCCATGTTTGATGTATCT
B2M	TCTCTGCTCCCCACCTCTAAGT
WDR3	CAAGTCGAGTGAGCTGGAAG
WDR3	AGGCACCGGCATATAAGTTC
WDR33	AGAGAGGCCAGTTTCTCACC
WDR33	TCATGGCAACGAAGAAAGTC
WDR21A	TGGATTCCCACATTCTGCTA
WDR21A	CGGTCTATTCCTGGGTGACT
WDR71	TGCTTGGGACTACAGAGCAG
WDR71	ACAGCAGTTGAAAGCGTCTG
p27	GCCCGGCGGCGCCTTTAATT
p27	GAAGAATCGTCGGTTGCAGGTCGCT

References

1.   Sharma, R.P., *Wingless--A new mutant in Drosophila melanogaster.* Dros. Inf. Serv., 1973. **50**: p. 134.

2.   C, N.-V. and W. E, *Mutations affecting segment number and polarity in Drosophila.* Nature, 1980: p. 795-801.

3.   Nusse, R. and H.E. Varmus, *Many tumors induced by the mouse mammary tumor virus contain a provirus integrated in the same region of the host genome.* Cell, 1982. **31**(1): p. 99-109.

4.   McMahon, A.P. and R.T. Moon, *Ectopic expression of the proto-oncogene int-1 in Xenopus embryos leads to duplication of the embryonic axis.* Cell, 1989. **58**(6): p. 1075-84.

5.   Holstein, T.W., *The evolution of the Wnt pathway.* Cold Spring Harb Perspect Biol, 2012. **4**(7): p. 7922.

6.   Sidow, A., *Diversification of the Wnt gene family on the ancestral lineage of vertebrates.* Proc Natl Acad Sci U S A, 1992. **89**(11): p. 5098-102.

7.   Gubb, D. and A. Garcia-Bellido, *A genetic analysis of the determination of cuticular polarity during development in Drosophila melanogaster.* J Embryol Exp Morphol, 1982. **68**: p. 37-57.

8.   Vinson, C.R., S. Conover, and P.N. Adler, *A Drosophila tissue polarity locus encodes a protein containing seven potential transmembrane domains.* Nature, 1989. **338**(6212): p. 263-4.

9.   Tomlinson, A., W.R. Strapps, and J. Heemskerk, *Linking Frizzled and Wnt signaling in Drosophila development.* Development, 1997. **124**(22): p. 4515-21.

10.   Rubinfeld, B., et al., *Association of the APC gene product with beta-catenin.* Science, 1993. **262**(5140): p. 1731-4.

11.   Ozawa, M., H. Baribault, and R. Kemler, *The cytoplasmic domain of the cell adhesion molecule uvomorulin associates with three independent proteins structurally related in different species.* EMBO J, 1989. **8**(6): p. 1711-7.

12.   Peifer, M. and E. Wieschaus, *The segment polarity gene armadillo encodes a functionally modular protein that is the Drosophila homolog of human plakoglobin.* Cell, 1990. **63**(6): p. 1167-76.

13. Pinson, K.I., et al., *An LDL-receptor-related protein mediates Wnt signalling in mice.* Nature, 2000. **407**(6803): p. 535-8.

14. Tamai, K., et al., *A mechanism for Wnt coreceptor activation.* Mol Cell, 2004. **13**(1): p. 149-56.

15. MacDonald, B.T., K. Tamai, and X. He, *Wnt/beta-catenin signaling: components, mechanisms, and diseases.* Dev Cell, 2009. **17**(1): p. 9-26.

16. Lindvall, C., et al., *Wnt signaling, stem cells, and the cellular origin of breast cancer.* Stem Cell Rev, 2007. **3**(2): p. 157-68.

17. Nusse, R. and H. Varmus, *Three decades of Wnts: a personal perspective on how a scientific field developed.* EMBO J, 2012. **31**(12): p. 2670-84.

18. Eisenmann, D.M., *Wnt signaling*, in *Wormbook*, T.C.E.R. Community, Editor. 2005, Wormbook.

19. Behrens, J., et al., *Functional interaction of beta-catenin with the transcription factor LEF-1.* Nature, 1996. **382**(6592): p. 638-42.

20. Albuquerque, C., et al., *Colorectal cancers show distinct mutation spectra in members of the canonical WNT signaling pathway according to their anatomical location and type of genetic instability.* Genes Chromosomes Cancer. **49**(8): p. 746-59.

21. Nagase, H. and Y. Nakamura, *Mutations of the APC (adenomatous polyposis coli) gene.* Hum Mutat, 1993. **2**(6): p. 425-34.

22. Groden, J., et al., *Identification and characterization of the familial adenomatous polyposis coli gene.* Cell, 1991. **66**(3): p. 589-600.

23. Su, L.K., et al., *Multiple intestinal neoplasia caused by a mutation in the murine homolog of the APC gene.* Science, 1992. **256**(5057): p. 668-70.

24. Korinek, V., et al., *Constitutive transcriptional activation by a beta-catenin-Tcf complex in APC-/- colon carcinoma.* Science, 1997. **275**(5307): p. 1784-7.

25. Satoh, S., et al., *AXIN1 mutations in hepatocellular carcinomas, and growth suppression in cancer cells by virus-mediated transfer of AXIN1.* Nat Genet, 2000. **24**(3): p. 245-50.

26. Anastas, J.N. and R.T. Moon, *WNT signalling pathways as therapeutic targets in cancer.* Nat Rev Cancer, 2013. **13**(1): p. 11-26.

27.   Wong, G.T., B.J. Gavin, and A.P. McMahon, *Differential transformation of mammary epithelial cells by Wnt genes.* Mol Cell Biol, 1994. **14**(9): p. 6278-86.

28.   Yoshioka, S., et al., *WNT7A regulates tumor growth and progression in ovarian cancer through the WNT/beta-catenin pathway.* Mol Cancer Res, 2012. **10**(3): p. 469-82.

29.   Ochoa-Hernandez, A.B., et al., *Peripheral T-lymphocytes express WNT7A and its restoration in leukemia-derived lymphoblasts inhibits cell proliferation.* BMC Cancer, 2012. **12**: p. 60.

30.   Carmon, K.S. and D.S. Loose, *Secreted frizzled-related protein 4 regulates two Wnt7a signaling pathways and inhibits proliferation in endometrial cancer cells.* Mol Cancer Res, 2008. **6**(6): p. 1017-28.

31.   Natarajan, K., et al., *Role of breast cancer resistance protein (BCRP/ABCG2) in cancer drug resistance.* Biochem Pharmacol, 2012. **83**(8): p. 1084-103.

32.   Valenta, T., et al., *Probing transcription-specific outputs of beta-catenin in vivo.* Genes Dev, 2011. **25**(24): p. 2631-43.

33.   Brembeck, F.H., et al., *BCL9-2 promotes early stages of intestinal tumor progression.* Gastroenterology, 2011. **141**(4): p. 1359-70, 1370 e1-3.

34.   Yu, Y., et al., *Kindlin 2 forms a transcriptional complex with beta-catenin and TCF4 to enhance Wnt signalling.* EMBO Rep, 2012. **13**(8): p. 750-8.

35.   Hoffmeyer, K., et al., *Wnt/beta-catenin signaling regulates telomerase in stem cells and cancer cells.* Science, 2012. **336**(6088): p. 1549-54.

36.   Collins, K. and J.R. Mitchell, *Telomerase in the human organism.* Oncogene, 2002. **21**(4): p. 564-79.

37.   Varshavsky, A., *The ubiquitin system, an immense realm.* Annu Rev Biochem, 2012. **81**: p. 167-76.

38.   Schulman, B.A. and J.W. Harper, *Ubiquitin-like protein activation by E1 enzymes: the apex for downstream signalling pathways.* Nat Rev Mol Cell Biol, 2009. **10**(5): p. 319-31.

39.   Yee, D. and D.R. Goring, *The diversity of plant U-box E3 ubiquitin ligases: from upstream activators to downstream target substrates.* J Exp Bot, 2009. **60**(4): p. 1109-21.

40.   Komander, D. and M. Rape, *The ubiquitin code.* Annu Rev Biochem, 2012. **81**: p. 203-29.

41.	Haglund, K., et al., *Multiple monoubiquitination of RTKs is sufficient for their endocytosis and degradation.* Nat Cell Biol, 2003. **5**(5): p. 461-6.

42.	Isasa, M., A. Zuin, and B. Crosas, *Integration of multiple ubiquitin signals in proteasome regulation.* Methods Mol Biol. **910**: p. 337-70.

43.	Attaix, D., et al., *Regulation of proteolysis.* Curr Opin Clin Nutr Metab Care, 2001. **4**(1): p. 45-9.

44.	Chen, J. and Z.J. Chen, *Regulation of NF-kappaB by ubiquitination.* Curr Opin Immunol. **25**(1): p. 4-12.

45.	Willis, M.S., et al., *Sent to destroy: the ubiquitin proteasome system regulates cell signaling and protein quality control in cardiovascular development and disease.* Circ Res. **106**(3): p. 463-78.

46.	Kaganovich, D., R. Kopito, and J. Frydman, *Misfolded proteins partition between two distinct quality control compartments.* Nature, 2008. **454**(7208): p. 1088-95.

47.	Harper, J.W. and B.A. Schulman, *Structural complexity in ubiquitin recognition.* Cell, 2006. **124**(6): p. 1133-6.

48.	Wakabayashi, K., et al., *The Lewy body in Parkinson's disease and related neurodegenerative disorders.* Mol Neurobiol, 2013. **47**(2): p. 495-508.

49.	Szargel, R., R. Rott, and S. Engelender, *Synphilin-1 isoforms in Parkinson's disease: regulation by phosphorylation and ubiquitylation.* Cell Mol Life Sci, 2008. **65**(1): p. 80-8.

50.	Rock, K.L., et al., *Inhibitors of the proteasome block the degradation of most cell proteins and the generation of peptides presented on MHC class I molecules.* Cell, 1994. **78**(5): p. 761-71.

51.	Winston, J.T., et al., *The SCFbeta-TRCP-ubiquitin ligase complex associates specifically with phosphorylated destruction motifs in IkappaBalpha and beta-catenin and stimulates IkappaBalpha ubiquitination in vitro.* Genes Dev, 1999. **13**(3): p. 270-83.

52.	Chitalia, V., et al., *c-Cbl, a ubiquitin E3 ligase that targets active beta-catenin - A novel layer of Wnt regulation.* J Biol Chem, 2013.

53.	Hay-Koren, A., et al., *The EDD E3 ubiquitin ligase ubiquitinates and up-regulates beta-catenin.* Mol Biol Cell, 2011. **22**(3): p. 399-411.

54.   Ding, Y., et al., *HECT domain-containing E3 ubiquitin ligase NEDD4L negatively regulates Wnt signaling by targeting dishevelled for proteasomal degradation.* J Biol Chem, 2013. **288**(12): p. 8289-98.

55.   Wei, W., et al., *The E3 ubiquitin ligase ITCH negatively regulates canonical Wnt signaling by targeting dishevelled protein.* Mol Cell Biol, 2012. **32**(19): p. 3903-12.

56.   Angers, S., et al., *The KLHL12-Cullin-3 ubiquitin ligase negatively regulates the Wnt-beta-catenin pathway by targeting Dishevelled for degradation.* Nat Cell Biol, 2006. **8**(4): p. 348-57.

57.   Lin, S.Y., et al., *Beta-catenin, a novel prognostic marker for breast cancer: its roles in cyclin D1 expression and cancer progression.* Proc Natl Acad Sci U S A, 2000. **97**(8): p. 4262-6.

58.   Lane, T.F. and P. Leder, *Wnt-10b directs hypermorphic development and transformation in mammary glands of male and female mice.* Oncogene, 1997. **15**(18): p. 2133-44.

59.   Bui, T.D., et al., *A novel human Wnt gene, WNT10B, maps to 12q13 and is expressed in human breast carcinomas.* Oncogene, 1997. **14**(10): p. 1249-53.

60.   Yu, Q., Y. Geng, and P. Sicinski, *Specific protection against breast cancers by cyclin D1 ablation.* Nature, 2001. **411**(6841): p. 1017-21.

61.   Anders, C.K. and L.A. Carey, *Biology, metastatic patterns, and treatment of patients with triple-negative breast cancer.* Clin Breast Cancer, 2009. **9 Suppl 2**: p. S73-81.

62.   Geyer, F.C., et al., *beta-Catenin pathway activation in breast cancer is associated with triple-negative phenotype but not with CTNNB1 mutation.* Mod Pathol. **24**(2): p. 209-31.

63.   King, T.D., M.J. Suto, and Y. Li, *The Wnt/beta-catenin signaling pathway: a potential therapeutic target in the treatment of triple negative breast cancer.* J Cell Biochem. **113**(1): p. 13-8.

64.   O'Toole, S.A., et al., *Therapeutic targets in triple negative breast cancer.* J Clin Pathol.

65.   Lindvall, C., et al., *The Wnt co-receptor Lrp6 is required for normal mouse mammary gland development.* PLoS One, 2009. **4**(6): p. e5813.

66.   Liu, C.C., et al., *LRP6 overexpression defines a class of breast cancer subtype and is a target for therapy.* Proc Natl Acad Sci U S A. **107**(11): p. 5136-41.

67.   Reya, T. and H. Clevers, *Wnt signalling in stem cells and cancer.* Nature, 2005. **434**(7035): p. 843-50.

68.   Liu, B.Y., et al., *The transforming activity of Wnt effectors correlates with their ability to induce the accumulation of mammary progenitor cells.* Proc Natl Acad Sci U S A, 2004. **101**(12): p. 4158-63.

69.   Kossatz, U. and N.P. Malek, *p27: tumor suppressor and oncogene.* Cell Res, 2007. **17**(10): p. 832-3.

70.   Miranda-Carboni, G.A., et al., *A functional link between Wnt signaling and SKP2-independent p27 turnover in mammary tumors.* Genes Dev, 2008. **22**(22): p. 3121-34.

71.   Pagano, M., et al., *Role of the ubiquitin-proteasome pathway in regulating abundance of the cyclin-dependent kinase inhibitor p27.* Science, 1995. **269**(5224): p. 682-5.

72.   Coats, S., et al., *Requirement of p27Kip1 for restriction point control of the fibroblast cell cycle.* Science, 1996. **272**(5263): p. 877-80.

73.   Hara, T., et al., *Role of the UBL-UBA protein KPC2 in degradation of p27 at G1 phase of the cell cycle.* Mol Cell Biol, 2005. **25**(21): p. 9292-303.

74.   Ishida, N., et al., *Phosphorylation of p27Kip1 on serine 10 is required for its binding to CRM1 and nuclear export.* J Biol Chem, 2002. **277**(17): p. 14355-8.

75.   Carrano, A.C., et al., *SKP2 is required for ubiquitin-mediated degradation of the CDK inhibitor p27.* Nat Cell Biol, 1999. **1**(4): p. 193-9.

76.   Malek, N.P., et al., *A mouse knock-in model exposes sequential proteolytic pathways that regulate p27Kip1 in G1 and S phase.* Nature, 2001. **413**(6853): p. 323-7.

77.   Nakayama, K., et al., *Targeted disruption of Skp2 results in accumulation of cyclin E and p27(Kip1), polyploidy and centrosome overduplication.* EMBO J, 2000. **19**(9): p. 2069-81.

78.   Kossatz, U., et al., *Skp2-dependent degradation of p27kip1 is essential for cell cycle progression.* Genes Dev, 2004. **18**(21): p. 2602-7.

79.   Traub, F., et al., *Prognostic impact of Skp2 and p27 in human breast cancer.* Breast Cancer Res Treat, 2006. **99**(2): p. 185-91.

80.   Livak, K.J. and T.D. Schmittgen, *Analysis of relative gene expression data using real-time quantitative PCR and the 2(-Delta Delta C(T)) Method.* Methods, 2001. **25**(4): p. 402-8.

81.   Chu, I., et al., *p27 phosphorylation by Src regulates inhibition of cyclin E-Cdk2.* Cell, 2007. **128**(2): p. 281-94.

82.   Belsches-Jablonski, A.P., et al., *Src family kinases and HER2 interactions in human breast cancer cell growth and survival.* Oncogene, 2001. **20**(12): p. 1465-75.

83.   Freland, L. and J.M. Beaulieu, *Inhibition of GSK3 by lithium, from single molecules to signaling networks.* Front Mol Neurosci, 2012. **5**: p. 14.

84.   Malhi, G.S., et al., *Potential mechanisms of action of lithium in bipolar disorder. Current understanding.* CNS Drugs, 2013. **27**(2): p. 135-53.

85.   Lustig, B., et al., *Negative feedback loop of Wnt signaling through upregulation of conductin/axin2 in colorectal and liver tumors.* Mol Cell Biol, 2002. **22**(4): p. 1184-93.

86.   Larrea, M.D., et al., *Phosphorylation of p27Kip1 regulates assembly and activation of cyclin D1-Cdk4.* Mol Cell Biol, 2008. **28**(20): p. 6462-72.

87.   Hao, B., et al., *Structural basis of the Cks1-dependent recognition of p27(Kip1) by the SCF(Skp2) ubiquitin ligase.* Mol Cell, 2005. **20**(1): p. 9-19.

88.   Frontini, M., et al., *The CDK subunit CKS2 counteracts CKS1 to control cyclin A/CDK2 activity in maintaining replicative fidelity and neurodevelopment.* Dev Cell, 2012. **23**(2): p. 356-70.

89.   Tan, M.K., H.J. Lim, and J.W. Harper, *SCF(FBXO22) regulates histone H3 lysine 9 and 36 methylation levels by targeting histone demethylase KDM4A for ubiquitin-mediated proteasomal degradation.* Mol Cell Biol. **31**(18): p. 3687-99.

90.   Spaich, S., et al., *F-box and leucine-rich repeat protein 22 is a cardiac-enriched F-box protein that regulates sarcomeric protein turnover and is essential for maintenance of contractile function in vivo.* Circ Res. **111**(12): p. 1504-16.

91.   Lavoie, J.N., et al., *Cyclin D1 expression is regulated positively by the p42/p44MAPK and negatively by the p38/HOGMAPK pathway.* J Biol Chem, 1996. **271**(34): p. 20608-16.

92.   Jacobi, C.L., et al., *Transcriptional regulation by the wilms tumor protein, wt1, suggests a role of the metalloproteinase adamts16 in murine genitourinary development.* J Biol Chem. **288**(26): p. 18811-24.

93.   Ahn, J.E., et al., *Insight into hypoxia tolerance in cowpea bruchid: metabolic repression and heat shock protein regulation via hypoxia-inducible factor 1.* PLoS One. **8**(4): p. e57267.

94.   Kamura, T., et al., *Cytoplasmic ubiquitin ligase KPC regulates proteolysis of p27(Kip1) at G1 phase.* Nat Cell Biol, 2004. **6**(12): p. 1229-35.

95.   Borziak, K. and I.B. Zhulin, *FIST: a sensory domain for diverse signal transduction pathways in prokaryotes and ubiquitin signaling in eukaryotes.* Bioinformatics, 2007. **23**(19): p. 2518-21.

96.   Havens, C.G., et al., *Direct role for proliferating cell nuclear antigen in substrate recognition by the E3 ubiquitin ligase CRL4Cdt2.* J Biol Chem. **287**(14): p. 11410-21.

97.   Ganoth, D., et al., *The cell-cycle regulatory protein Cks1 is required for SCF(Skp2)-mediated ubiquitinylation of p27.* Nat Cell Biol, 2001. **3**(3): p. 321-4.

98.   Nusse, R. and H.E. Varmus, *Wnt genes.* Cell, 1992. **69**(7): p. 1073-87.

99.   Suraweera, N., et al., *Mutations within Wnt pathway genes in sporadic colorectal cancers and cell lines.* Int J Cancer, 2006. **119**(8): p. 1837-42.

100.   Nakamura, Y., et al., *Mutations of the APC (adenomatous polyposis coli) gene in FAP (familial polyposis coli) patients and in sporadic colorectal tumors.* Tohoku J Exp Med, 1992. **168**(2): p. 141-7.

101.   Nakatsuru, S., et al., *Somatic mutation of the APC gene in gastric cancer: frequent mutations in very well differentiated adenocarcinoma and signet-ring cell carcinoma.* Hum Mol Genet, 1992. **1**(8): p. 559-63.

102.   Scholer-Dahirel, A. and M.E. McLaughlin, *Determinants of Wnt/beta-catenin pathway dependency in colorectal cancer.* Cell Cycle. **11**(1): p. 9-10.

103.   Verras, M. and Z. Sun, *Roles and regulation of Wnt signaling and beta-catenin in prostate cancer.* Cancer Lett, 2006. **237**(1): p. 22-32.

104.   Zheng, N., et al., *Structure of the Cul1-RBX1-Skp1-F boxSkp2 SCF ubiquitin ligase complex.* Nature, 2002. **416**(6882): p. 703-9.

105.   Higa, L.A. and H. Zhang, *Stealing the spotlight: CUL4-DDB1 ubiquitin ligase docks WD40-repeat proteins to destroy.* Cell Div, 2007. **2**: p. 5.

106.   Angers, S., et al., *Molecular architecture and assembly of the DDB1-CUL4A ubiquitin ligase machinery.* Nature, 2006. **443**(7111): p. 590-3.

107.   Abbas, T. and A. Dutta, *p21 in cancer: intricate networks and multiple activities.* Nat Rev Cancer, 2009. **9**(6): p. 400-14.

108.   Jin, J., et al., *A family of diverse CUL4-Ddb1-interacting proteins includes Cdt2, which is required for S phase destruction of the replication factor Cdt1.* Mol Cell, 2006. **23**(5): p. 709-21.

109.   Higa, L.A., et al., *L2DTL/CDT2 interacts with the CUL4/DDB1 complex and PCNA and regulates CDT1 proteolysis in response to DNA damage.* Cell Cycle, 2006. **5**(15): p. 1675-80.

110.   Xu, H., et al., *DCAF26, an adaptor protein of CUL4-based E3, is essential for DNA methylation in Neurospora crassa.* PLoS Genet. **6**(9): p. e1001132.

111.   Abbas, T., et al., *PCNA-dependent regulation of p21 ubiquitylation and degradation via the CRL4Cdt2 ubiquitin ligase complex.* Genes Dev, 2008. **22**(18): p. 2496-506.

112.   Hoverter, N.P., et al., *A WNT/p21 circuit directed by the C-clamp, a sequence-specific DNA binding domain in TCFs.* Mol Cell Biol, 2012. **32**(18): p. 3648-62.

113.   Liu, H. and J.H. Naismith, *An efficient one-step site-directed deletion, insertion, single and multiple-site plasmid mutagenesis protocol.* BMC Biotechnol, 2008. **8**: p. 91.

114.   Wolters, D.A., M.P. Washburn, and J.R. Yates, 3rd, *An automated multidimensional protein identification technology for shotgun proteomics.* Anal Chem, 2001. **73**(23): p. 5683-90.

115.   Florens, L., et al., *Analyzing chromatin remodeling complexes using shotgun proteomics and normalized spectral abundance factors.* Methods, 2006. **40**(4): p. 303-11.

116.   Washburn, M.P., D. Wolters, and J.R. Yates, 3rd, *Large-scale analysis of the yeast proteome by multidimensional protein identification technology.* Nat Biotechnol, 2001. **19**(3): p. 242-7.

117.   J. Eng, A.M., J. Yates, *An approach to correlate tandem mass spectral data of peptides with amino acid sequences in a protein database.* J Am Soc Mass Spectrom, 1994. **5**(11): p. 976.

118.   Tabb, D.L., W.H. McDonald, and J.R. Yates, 3rd, *DTASelect and Contrast: tools for assembling and comparing protein identifications from shotgun proteomics.* J Proteome Res, 2002. **1**(1): p. 21-6.

119.   Wohlschlegel, J.A., *Identification of SUMO-conjugated proteins and their SUMO attachment sites using proteomic mass spectrometry.* Methods Mol Biol, 2009. **497**: p. 33-49.

120.   Shen, K.C., et al., *Isolation and characterization of a breast progenitor epithelial cell line with robust DNA damage responses.* Breast Cancer Res Treat, 2006. **98**(3): p. 357-64.

121.   Rost, B., G. Yachdav, and J. Liu, *The PredictProtein server.* Nucleic Acids Res, 2004. **32**(Web Server issue): p. W321-6.

122.   Xu, D., A. Farmer, and Y.M. Chook, *Recognition of nuclear targeting signals by Karyopherin-beta proteins.* Curr Opin Struct Biol, 2010. **20**(6): p. 782-90.

123.   Fischer, E.S., et al., *The molecular basis of CRL4DDB2/CSA ubiquitin ligase architecture, targeting, and activation.* Cell, 2011. **147**(5): p. 1024-39.

124.   Liggett, W.H., Jr. and D. Sidransky, *Role of the p16 tumor suppressor gene in cancer.* J Clin Oncol, 1998. **16**(3): p. 1197-206.

125.   Shapiro, G.I., et al., *p16INK4A participates in a G1 arrest checkpoint in response to DNA damage.* Mol Cell Biol, 1998. **18**(1): p. 378-87.

126.   Yoneda-Kato, N. and J.Y. Kato, *Shuttling imbalance of MLF1 results in p53 instability and increases susceptibility to oncogenic transformation.* Mol Cell Biol, 2008. **28**(1): p. 422-34.

127.   Zhuge, C., et al., *PDCD5-regulated cell fate decision after ultraviolet-irradiation-induced DNA damage.* Biophys J, 2011. **101**(11): p. 2582-91.

128.   Du, Y.J., et al., *Reduced expression of programmed cell death 5 protein in tissue of human prostate cancer.* Chin Med Sci J, 2009. **24**(4): p. 241-5.

129.   Zhang, X., et al., *Clinical and prognostic significance of lost or decreased PDCD5 expression in human epithelial ovarian carcinomas.* Oncol Rep, 2011. **25**(2): p. 353-8.

130.   Kotake, Y., Y. Zeng, and Y. Xiong, DDB*1-CUL4 and MLL1 mediate oncogene-induced p16INK4a activation.* Cancer Res, 2009. **69**(5): p. 1809-14.

131.   Desmots, F., et al., *Scythe regulates apoptosis-inducing factor stability during endoplasmic reticulum stress-induced apoptosis.* J Biol Chem, 2008. **283**(6): p. 3264-71.

132. Roberts, D.M., et al., *Defining components of the beta-catenin destruction complex and exploring its regulation and mechanisms of action during development.* PLoS One, 2012. **7**(2): p. e31284.

133. van Noort, M., et al., *Wnt signaling controls the phosphorylation status of beta-catenin.* J Biol Chem, 2002. **277**(20): p. 17901-5.

134. Rao, A.S., et al., *Lithium stimulates proliferation in cultured thyrocytes by activating Wnt/beta-catenin signalling.* Eur J Endocrinol, 2005. **153**(6): p. 929-38.

135. Higa, L.A., et al., *CUL4-DDB1 ubiquitin ligase interacts with multiple WD40-repeat proteins and regulates histone methylation.* Nat Cell Biol, 2006. **8**(11): p. 1277-83.

136. Woo, J.L. and A.J. Berk, *Adenovirus ubiquitin-protein ligase stimulates viral late mRNA nuclear export.* J Virol, 2007. **81**(2): p. 575-87.

137. Sowa, M.E., et al., *Defining the human deubiquitinating enzyme interaction landscape.* Cell, 2009. **138**(2): p. 389-403.

138. Choi, H.H., et al., *COP9 signalosome subunit 6 stabilizes COP1, which functions as an E3 ubiquitin ligase for 14-3-3sigma.* Oncogene, 2011. **30**(48): p. 4791-801.

139. He, Y.J., et al., DDB*1 functions as a linker to recruit receptor WD40 proteins to CUL4-ROC1 ubiquitin ligases.* Genes Dev, 2006. **20**(21): p. 2949-54.

140. Vainberg, I.E., et al., *Prefoldin, a chaperone that delivers unfolded proteins to cytosolic chaperonin.* Cell, 1998. **93**(5): p. 863-73.

141. Whitehead, T.A., et al., *A filamentous molecular chaperone of the prefoldin family from the deep-sea hyperthermophile Methanocaldococcus jannaschii.* Protein Sci, 2007. **16**(4): p. 626-34.

142. Mousnier, A., et al., *von Hippel Lindau binding protein 1-mediated degradation of integrase affects HIV-1 gene expression at a postintegration step.* Proc Natl Acad Sci U S A, 2007. **104**(34): p. 13615-20.

143. Delgehyr, N., et al., *Drosophila Mgr, a Prefoldin subunit cooperating with von Hippel Lindau to regulate tubulin stability.* Proc Natl Acad Sci U S A. **109**(15): p. 5729-34.

144. Kopanja, D., et al., *CUL4A is essential for spermatogenesis and male fertility.* Dev Biol, 2011. **352**(2): p. 278-87.

145.   Xu, Y., et al., *A Ubiquitin-like Domain Recruits an Oligomeric Chaperone to a Retrotranslocation Complex in Endoplasmic Reticulum-associated Degradation.* J Biol Chem, 2013. **288**(25): p. 18068-76.

146.   Claessen, J.H. and H.L. Ploegh, *BAT3 guides misfolded glycoproteins out of the endoplasmic reticulum.* PLoS One, 2011. **6**(12): p. 28542.

147.   Leznicki, P., et al., *Bat3 promotes the membrane integration of tail-anchored proteins.* J Cell Sci, 2010. **123**(Pt 13): p. 2170-8.

148.   Kawahara, H., R. Minami, and N. Yokota, *BAG6/BAT3: emerging roles in quality control for nascent polypeptides.* J Biochem, 2013. **153**(2): p. 147-60.

149.   Minami, R., et al., *BAG-6 is essential for selective elimination of defective proteasomal substrates.* J Cell Biol, 2010. **190**(4): p. 637-50.

150.   Ensminger, A.W. and R.R. Isberg, *E3 ubiquitin ligase activity and targeting of BAT3 by multiple Legionella pneumophila translocated substrates.* Infect Immun, 2010. **78**(9): p. 3905-19.

151.   Desmots, F., et al., *The reaper-binding protein scythe modulates apoptosis and proliferation during mammalian development.* Mol Cell Biol, 2005. **25**(23): p. 10329-37.

152.   Wu, Y.H., S.F. Shih, and J.Y. Lin, *Ricin triggers apoptotic morphological changes through caspase-3 cleavage of BAT3.* J Biol Chem, 2004. **279**(18): p. 19264-75.

153.   Abu-Zant, A., et al., *Incomplete activation of macrophage apoptosis during intracellular replication of Legionella pneumophila.* Infect Immun, 2005. **73**(9): p. 5339-49.

154.   Lehner, B., et al., *Analysis of a high-throughput yeast two-hybrid system and its use to predict the function of intracellular proteins encoded within the human MHC class III region.* Genomics, 2004. **83**(1): p. 153-67.

155.   Kitagawa, K., et al., *SGT1 encodes an essential component of the yeast kinetochore assembly pathway and a novel subunit of the SCF ubiquitin ligase complex.* Mol Cell, 1999. **4**(1): p. 21-33.

156.   Mayor, A., et al., *A crucial function of SGT1 and HSP90 in inflammasome activity links mammalian and plant innate immune responses.* Nat Immunol, 2007. **8**(5): p. 497-503.

157.   Wei, W., et al., *Degradation of the SCF component Skp2 in cell-cycle phase G1 by the anaphase-promoting complex.* Nature, 2004. **428**(6979): p. 194-8.

158.   Liu, W., et al., *Cdh1-anaphase-promoting complex targets Skp2 for destruction in transforming growth factor beta-induced growth inhibition.* Mol Cell Biol, 2007. **27**(8): p. 2967-79.

159.   Kamper, N., et al., *A novel BAT3 sequence generated by alternative RNA splicing of exon 11B displays cell type-specific expression and impacts on subcellular localization.* PLoS One, 2012. **7**(4): p. 35972.

160.   Sasaki, T., et al., *Bat3 deficiency accelerates the degradation of Hsp70-2/HspA2 during spermatogenesis.* J Cell Biol, 2008. **182**(3): p. 449-58.